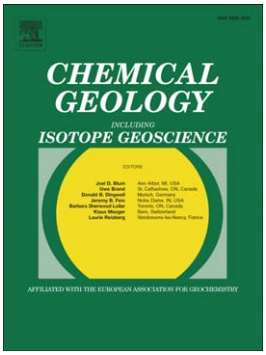

Tracing the effects of high-pressure metasomatic fluids and seawater alteration in blueschist-facies overprinted eclogites: Implications for subduction channel processes

François van der Straaten, Ralf Halama, Timm John, Volker Schenk, Folkmar Hauff, Nils Andersen

PII: S0009-2541(11)00444-X
DOI: doi: 10.1016/j.chemgeo.2011.11.008
Reference: CHEMGE 16353

To appear in: *Chemical Geology*

Received date: 22 December 2010
Revised date: 7 November 2011
Accepted date: 8 November 2011

Please cite this article as: der Straaten, François van, Halama, Ralf, John, Timm, Schenk, Volker, Hauff, Folkmar, Andersen, Nils, Tracing the effects of high-pressure metasomatic fluids and seawater alteration in blueschist-facies overprinted eclogites: Implications for subduction channel processes, *Chemical Geology* (2011), doi: 10.1016/j.chemgeo.2011.11.008

Tracing the effects of high-pressure metasomatic fluids and seawater alteration in blueschist-facies overprinted eclogites: Implications for subduction channel processes

François van der Straaten[a], Ralf Halama[a,*], Timm John[b], Volker Schenk[a], Folkmar Hauff[c], Nils Andersen[d]

[a] SFB 574 and Institut für Geowissenschaften, Universität Kiel, Ludewig-Meyn-Str. 10, 24118 Kiel, Germany

[b] Institut für Mineralogie, Universität Münster, Corrensstr. 24, 48149 Münster, Germany

[c] SFB 574 and IFM-GEOMAR, Wischhofstr. 1-3, 24148 Kiel, Germany

[d] Leibniz Laboratory for Radiometric Dating and Stable Isotope Research, Universität Kiel, Max-Eyth-Str. 11, 24148 Kiel, Germany

* Corresponding author contact information:

Ralf Halama

Institut für Geowissenschaften and SFB 574

Universität Kiel, 24098 Kiel, Germany

E-mail: *rh@min.uni-kiel.de*

Tel: +49-431-880-1911

Fax: +49-431-880-4457

Abstract

Eclogites from the Tian Shan high-pressure/low-temperature (HP/LT) metamorphic belt show evidence for successively increasing metasomatic alteration with increasing retrograde, blueschist-facies overprint. To constrain the source(s) of the metasomatizing fluid and to evaluate elemental and isotopic changes during this overprint, two sequences of eclogite-blueschist transitions were investigated: A layered transition from eclogite to blueschist (FTS 9-1 sequence) and blueschist-facies overprinted pillow metabasalts (FTS 4 samples).

Geochemical trends based on the relationships of K, Ba, Rb and Th are consistent with HP metasomatism, but distinct from typical seafloor alteration trends. In contrast, oxygen isotope ratios in garnet ($\delta^{18}O_{V\text{-}SMOW}$ = 7.3–8.7‰) and omphacite ($\delta^{18}O_{V\text{-}SMOW}$ = 8.2–9.7‰) are similar to $\delta^{18}O_{V\text{-}SMOW}$ in bulk low-temperature altered oceanic crust (AOC), suggesting O isotopic preservation of a seafloor alteration signature. Carbonate crystallization related to the metasomatic overprint demonstrate CO_2 mobility during subduction and potential C storage in HP metamorphic rocks. Carbon isotope ratios in the two sequences differ markedly: Disseminated calcite in the layered FTS 9-1 sequence has $\delta^{13}C_{V\text{-}PDB}$ = -9.14±0.19‰, whereas vein-forming ankerite in the pillow metabasalts has $\delta^{13}C_{V\text{-}PDB}$ = -2.08±0.12‰. The ankerite reflects an inorganic marine/hydrothermal signature, as observed in ophiolites, whereas the low $\delta^{13}C_{V\text{-}PDB}$ values from the calcite point to a contribution of organic carbon.

The time when the metasomatic overprint occurred is estimated to be ~320±11 Ma based on a Rb-Sr isochron age of six blueschist samples from the pillow metabasalts, which is in agreement with active subduction in this region. Initial (T=320 Ma) $^{87}Sr/^{86}Sr$ ratios for all HP/LT rocks range from 0.7059 – 0.7085, and εNd_{320Ma} varies from -0.4 to +10.9. Both eclogite-blueschist sequences have initial Sr isotope compositions ($^{87}Sr/^{86}Sr$ ~0.707) that are significantly higher than those of typical oceanic mantle-derived basalts. They are thought to derive from a fluid that preserved the Sr isotopic signature of seawater by fluid-rock interaction with seawater-altered oceanic lithosphere in a subduction channel. Mixing models between eclogite and various fluids suggest that the contribution of a sediment-derived fluid was likely less than 20%. A fluid predominantly derived from seawater-altered oceanic lithosphere is also supported by the calculated O isotope composition of the fluids (10.2 – 11.2‰). It is thus evident that subduction channel fluids carry complex, mixed elemental and isotopic signatures, which reflect the composition of their source rocks modified by interaction with various other lithologies.

Keywords: subduction, eclogite, metasomatism, seafloor alteration, Tian Shan;

1. INTRODUCTION

Fluids play an important role in many fundamental geological processes, including metamorphism and metasomatism in subduction zones (e.g., Austrheim, 1987; Bebout and Barton, 1993; Putnis and John, 2010) and the generation of arc magmas (e.g., Hawkesworth et al., 1993; Stolper and Newman, 1994; Tatsumi, 1989). The direct examination of subduction zone metamorphic rocks provides insights about slab-derived agents added to arc magma sources and about element mobility and material transport during the subduction cycle (e.g. Bebout, 2007; Beinlich et al., 2010; Breeding et al., 2004; John et al., 2004; Sorensen et al., 1997; Spandler et al., 2004).

Increasing attention has been directed towards metasomatic changes in subducted high-pressure (HP) rocks caused by fluids released from the subducted slab (e.g., Halama et al., 2011; Marschall et al., 2009; Miller et al., 2009; Penniston-Dorland et al., 2010) and by fluid-rock interaction in the subduction channel (Bebout and Barton, 1993; Horodyskyj et al., 2009; van der Straaten et al., 2008). The subduction channel is defined as the zone of partially serpentinized mantle peridotite between the down-going slab and the dry mantle wedge and develops by reaction of slab fluids with the mantle wedge peridotite (Cloos and Shreve, 1988; Gerya et al., 2002). These metasomatized rocks may constitute new bulk compositions that can influence the redistribution of major and trace elements (e.g., Bebout, 2007; King et al., 2006; Putnis and John, 2010; Scambelluri et al., 2006), which may be transported over short distances (redistribution on cm scale; e.g., Hermann, 2002; Spandler et al., 2003; Hermann et al., 2006) or long distances (removal from a system on outcrop scale; e.g., Gao et al., 2007; Zack and John, 2007; John et al., 2008; Spandler et al., 2011). Radiogenic and stable isotope studies in fluid-overprinted metamorphic rocks can provide information about the extent of fluid-rock interactions (e.g., Baker et al., 1997; Yui et al., 1997; Zheng et al., 1999) and the identification of potential fluid sources (e.g., Bebout and Barton, 1993; Halama et al., 2010, 2011; King et al., 2006; Scambelluri and Phillipot, 2001; Sadofsky and Bebout, 2004). In principle, fluids in the subduction zone may originate from (I) the partly serpentinised, subducted mantle peridotite underneath the oceanic crust (Hyndman and Peacock, 2003; Ranero et al., 2003), (II) the altered oceanic crust (AOC; e.g. Becker et al., 2000; John et al., 2008; Peacock, 1993), (III) subducted marine sediments (Plank and Langmuir, 1993; Rüpke et al., 2002), and (IV) the mélange zone of the slab-wedge interface (Bebout, 2007; King et al., 2006; Spandler et al., 2008). Fluids circulating in the subduction zone may inherit the

chemical and isotopic signatures of these reservoirs and may in addition get overprinted by the geochemical signature of the partly serpentinised peridotites of the mantle wedge (van der Straaten et al., 2008). It has also been demonstrated that fluids in HP metamorphic rocks play a key role in promoting equilibration of isotopic systems used as geochronometers (Glodny et al., 2003, 2008). In turn, some isotopic systems may still record the effects of previous seafloor alteration or the isotopic signature of the precursor rock (Halama et al., 2010, 2011; John et al., 2011; Miller et al., 1988; Putlitz et al., 2000).

Eclogites typically have a well-defined basaltic composition and mineral assemblages dominated by nominally anhydrous minerals. Thus, details about the fluid composition and fluid-induced metasomatic processes can be obtained from metasomatically transformed eclogites (Halama et al., 2011; Penniston-Dorland et al., 2010; van der Straaten et al., 2008). Here, two dm to m scale sequences from the Chinese Tian Shan HP belt, displaying gradual transitions from eclogite to retrograde blueschist, were investigated using C, O, Sr and Nd isotope data combined with mass-balance calculations to determine protolith compositions, elemental enrichments and depletions and to constrain the source of the metasomatizing fluid. The combination of several isotopic systems is used to discern between the effects of seafloor alteration and HP metasomatism and contributes to a better understanding of metasomatic processes during the subduction cycle.

2. GEOLOGY AND SAMPLE DESCRIPTION

The samples come from a belt of high-pressure, low-temperature (HP/LT) metamorphic rocks, which occurs in the Chinese part of the Tian Shan orogen (Fig. 1). The Tian Shan stretches from NW China to Kirghizia and Tajikistan and is situated along the southwestern margin of the Central Asia Orogenic Belt (Gao et al., 1995; Sengör et al., 1993; Volkova and Budanov, 1999). In the Chinese part of the South Tian Shan, the HP/LT belt extends along the Southern Central Tian Shan suture for at least 200 km, separating the Tarim craton to the south and the Yili – central Tian Shan block to the north. The belt represents a subduction/collision zone between Yili-Kazakhstan-Kyzylkum and Tarim-Karakum plates (Volkova and Budanov, 1999). The HP rocks are interpreted as relics of the Palaeozoic South Tian Shan Ocean basin, including former seamounts and young arcs, subducted during Silurian and Carboniferous time (Gao et al., 1998; Sengör and Natal'in, 1996; Windley et al., 1990; Gao and Klemd, 2003; Klemd et al., 2011). Lutetium–Hf ages of four high-pressure rocks overlap around 315 Ma and date high-pressure garnet growth (Klemd et al., 2011),

which combined with the ~311 Ma cluster of ^{40}Ar–^{39}Ar and Rb–Sr white mica ages (Klemd et al., 2005) from adjacent rocks imply fast exhumation rates (Klemd et al., 2011). The HP/LT sequences occur discontinuously within a Paleozoic accretionary wedge (Gao et al., 1995, 1998) and predominantly comprise eclogite-, blueschist-, and greenschist-facies metasedimentary rocks. Subordinate metavolcanic rocks, ultramafic slices and lenses of Silurian marble occur as exotic blocks and point towards an origin as tectonic mélange (Gao et al., 1999; van der Straaten et al., 2008). The blueschists occur as lenses, bands or layers within greenschist facies metasediments and are intercalated with pods (15-25 cm in diameter), boudins, layers (2-25 cm thickness) or large blocks (2 km^2) of eclogite (Gao et al., 1999). Blueschist occurrences include prograde and retrograde varieties (Gao and Klemd, 2001; Gao et al., 2007; van der Straaten et al., 2008; Beinlich et al., 2010). The retrograde blueschists are interpreted to have formed by fluid-rock interaction during uplift in the subduction channel (van der Straaten et al., 2008).

Gradual transitions between prograde blueschist and eclogite suggest that both have experienced identical peak metamorphic conditions of 480-580 °C, locally up to 700°C, at 1.4-2.1 GPa (Klemd et al., 2002; van der Straaten et al., 2008; Beinlich et al., 2010). UHP peak metamorphic conditions – confirmed by coesite - of 2.7 GPa at 420-520°C have been reported for one eclogite boudin (Lü et al., 2009), which occurs enclosed in HP and UHP mica-schist of variable peak metamorphic conditions. Their PT-values are ca. 3.2 GPa at 550-570°C, ca. 2.2 GPa at 550°C and ca. 2.3 GPa at 540 and 550°C, all of which have been derived by pseudosection modeling (Lü et al., 2008; Wei et al., 2009). However, other eclogite boudins from the same locality display PT-conditions of 1.8 – 2.5 GPa at 400 to 600°C (Lü et al., 2007). The occurrence of UHP and HP eclogite-facies rocks juxtaposed on a meter scale is interpreted to have resulted from mixing of eclogite-facies rock from different depths in the subduction channel (Lü et al., 2009), confirming the basic concept of van der Straaten et al. (2008). This scenario is supported by the fact that some of the Tian Shan eclogites define a P-T path of decompression associated with retrograde cooling (Gao et al., 1998; van der Straaten et al., 2008), which is characteristic for uplift in a subduction channel (Gerya et al., 2002).

Two different sequences comprising a gradual transition from eclogite to blueschist were investigated in this study: I) A lithologically layered sequence of eclogite that is laterally transformed to blueschist (sample sequence FTS 9-1; GPS coordinates: 42°31’48’’N, 81°21’30’’E; Fig. 2A). The eclogitic part of this sequence is bordered by a quartz-rich vein and a meta-acidite. II) Metabasalts with pillow structures (in the following labeled as “pillow

metabasalt") with eclogite-facies mineralogy preserved in the pillow cores showing marginal transformation to blueschist (samples FTS 4-1.1, 4-2.4, 4-3.3, 4-3.5; GPS coordinates: 42°28'59''N, 81°15'38''S; Fig. 2B). The FTS 4 samples were the subject of a petrologic and geochemical study by van der Straaten et al. (2008). For the profiles, drill cores with a diameter of 2.54 cm and a length of about 10-15 cm were taken to obtain a good spatial resolution. At both localities, the samples occur as loose, meter-sized blocks, which have fallen from the steep mountain slopes as rock falls. The in-situ outcrops are either covered by glaciers or occur on extremely steep walls and are not accessible. The blocks represent a mixture of various rock types that are now found within and partly covered by quaternary deposits.

Eclogites and blueschists of the FTS 9-1 sequence contain omphacite + garnet + rutile + phengite (partly Cr-rich) + paragonite + glaucophane + titanite ± calcite. The eclogitic parts consist of a fine-grained omphacite matrix with accessory rutile and porphyroblasts of garnet (Fig. 3a). Omphacite, amphibole, rutile, quartz, phengite and clinozoisite occur as inclusions in garnet. In the blueschist-facies overprinted parts, omphacite and garnet are replaced by newly formed glaucophane and paragonite (Fig. 3b). Titanite replaces rutile and grows poikiloblastically around matrix omphacite (van der Straaten, 2008). Calcite forms distinct aggregates in the matrix (Fig. 3b). Garnet is increasingly resorbed with increasing overprint and replaced by chlorite and calcite. The modal amounts of glaucophane, white mica and calcite increase with increasing blueschist-facies overprint leading to nearly complete replacement of omphacite in the pure blueschist sample (van der Straaten, 2008).

The mineral assemblage of the pillow metabasalts (FTS 4 series) is garnet + omphacite + clinozoisite + rutile + apatite in the eclogite parts. This assemblage was transformed by fluid-induced retrograde metamorphism from the pillow margins inwards, forming shells of phengite-ankerite blueschist (outer shell with phengite, glaucophane, ankerite and titanite as major mineral phases) and glaucophane-dominated blueschist (inner shell). A detailed study of the petrology as well as major and trace element geochemistry of the pillow metabasalts was presented by van der Straaten et al. (2008).

For a better evaluation of the geochemical and isotopic variations of the mélange rocks, several samples from other blocks and boulders were collected. These comprise two meta-igneous rocks, a coarse-grained eclogite (FTS 1-26) and a glaucophane schist (FTS 5-6), and two metasedimentary rocks, a garnet-mica-schist (FTS 2-15) and a fuchsite schist (FTS 6-5B).

3. ANALYTICAL METHODS

3.1 Major and trace elements

Whole rock major element contents of the FTS 9-1 sequence and associated mélange rocks were analyzed by XRF on fused glass discs with a Philips PW1480 XRF spectrometer at Kiel University (Table 1). The relative standard deviation (RSD) for all oxides is generally ≤ 1.3% based on multiple analyses of reference material BHVO-1 (see van der Straaten et al., 2008, for details on precision and accuracy). For the FTS-9 eclogite-blueschist sequence, concentrations of 38 trace elements were determined by inductively coupled plasma mass spectrometry (ICP-MS) using a Agilent 7500c instrument at Kiel University after HF-HNO_3-$HClO_4$ acid digestion in Teflon bombs at 180°C. Details about sample preparation and the analytical protocol are given by Garbe-Schönberg (1993) and John et al. (2008). Precision based on the RSD of reference material BHVO-2 and a representative sample solution measured 5 times is < 4% for most trace elements. Sample powder homogeneity and potential contamination during sample preparation were evaluated by duplicate analysis of an unknown, yielding RSD values <5% for all elements except Cr (RSD = 15%). Details about blank and reference material analyses for samples analyzed during the course of this study are given in van der Straaten et al. (2008). For the mélange rocks and the neighboring rocks of the FTS 9-1 sequence, 36 trace elements were analyzed by Acme Analytical Laboratories (Vancouver, Canada). REE and refractory elements were analyzed by ICP-MS following lithium metaborate fusion and nitric acid digestion, whereas base metals were analyzed by ICP-MS after Aqua Regia digestion. Detection limits are 0.01-0.3 ppm for REE, 0.1-0.2 ppm for HFSE, 0.1-8 ppm for transition metals and 0.1-1 ppm for LILE (see also http://acmelab.com/). During the course of this study, the standards SO-18, DS7 and OREAS45PA were analyzed for quality control. Precision based on repeat standard analysis (n=6) is <5% except for Ni (~8%) and Pb (~13%). All measured values were accurate to the expected values to about ± 6%, with slightly greater deviations for Sm (-10%) and Tb (-8%). Blank levels were below the detection limits for all elements except Zr (blank = 1.2 ppm).

3.2 C-O isotopes in carbonates

Carbon and oxygen isotopic ratios were analyzed at the Leibniz-Laboratory for Radiometric Dating and Stable Isotope Research (Kiel, Germany). Handpicked calcite and ankerite separates were treated with 100% phosphoric acid at 75°C in an automated carbonate preparation system (Kiel device) for 6 and 18 minutes, respectively. The liberated CO_2 gas

was analyzed with a Finnigan MAT 251 mass spectrometer using a dual inlet system. Carbon and oxygen isotope ratios are expressed in the standard δ notation in per mil (‰) relative to the international V-PDB and V-SMOW isotope standards, respectively. The $\delta^{13}C$ and $\delta^{18}O$ values of the carbonate carbon were calibrated against international standards (NBS 19; NBS 20) and several laboratory internal standards. The analytical uncertainty (1σ) is < ±0.05‰ for $\delta^{13}C$ and < ±0.07‰ for $\delta^{18}O$.

Since ankerite is not routinely analyzed for C- and O isotopes, completeness of reaction was tested by applying reaction times of 18, 26 and 34 minutes. From the ankerite vein sample 4-2.5, ankerite was separated and divided into 4 subsamples (4-2.5A to –D; see Table 2). The lack of clear systematic trends in $\delta^{13}C$ and $\delta^{18}O$ with increasing reaction time indicates that ankerite has fully reacted after 18 minutes and that sample inhomogeneities and/or effects of powdering have likely caused the minor differences just outside analytical uncertainty.

3.3 O isotopes in silicates

Oxygen isotope measurements of handpicked mineral separates were made at the Geowissenschaftliches Zentrum, University of Göttingen (Germany) using a laser fluorination method similar to that described by Sharp (1990). Details of the analytical protocol and the mass spectrometric measurements are described by Pack et al. (2007). In brief, 1-2 mg of the separated minerals are loaded in a Ni sample holder and evacuated overnight. Samples are melted with 50 W CO_2 laser (λ = 10.6 µm) and fluorinated with purified F_2 gas (~20 mbar). Excess F_2 reacts with heated NaCl (~150°C) to NaF and Cl_2 is trapped with liquid nitrogen at -196°C. The extracted O_2 is trapped on a 5Å molecular sieve at – 196°C before being transferred into the sample bellows of the spectrometer by heating up the molecular sieve to +80°C. Isotopic analyses of O_2 gas are carried out on a Finnigan Delta plus mass spectrometer, which is equipped with three Faraday cups with 3 x 10^8, 3 x 10^{11} and 1 x 10^{11} Ω feedback resistors for simultaneous measurement of oxygen with m/z 32, 33 and 34. A conventional dual inlet system with bottled reference O_2 of known $\delta^{18}O_{V\text{-}SMOW}$ (+12.5‰) was used. Results are reported as the per mil deviation from Vienna Standard Mean Ocean Water (V-SMOW) in the standard δ-notation. Measurements of the UWG-2 garnet reference material gave $\delta^{18}O$ = 5.66±0.08‰ (1σ, n=9), in good agreement with the reference value of +5.74±0.15‰ given by Valley et al. (1995). Based on long-term reproducibility, an analytical uncertainty (1σ) of ±0.2‰ is assumed for the samples analyzed in this study.

3.4 Sr-Nd isotopes

Strontium and Nd isotopic analyses were carried out at IFM-GEOMAR (Kiel, Germany), partly using sample solutions from ICP-MS trace element measurements and partly whole-rock powders. For the former, diluted HNO_3 solutions were evaporated and the sample matrix was converted into chloride form. New whole-rock powders were dissolved for 2 days in a 5:1 mixture of ultrapure HF and HNO_3 at 150°C. The ion exchange procedures followed those described in Hoernle and Tilton (1991). Isotopic ratios were determined in static multi-collection on a Finnigan MAT262 (Sr) and a Thermo-Finnigan TRITON (Nd) thermal ionization mass spectrometer (TIMS). Strontium and Nd isotopic ratios are normalized within run to $^{86}Sr/^{88}Sr = 0.1194$ and $^{146}Nd/^{144}Nd = 0.7219$. Reference material measured along with the samples during the two analytical periods of this study gave $^{87}Sr/^{86}Sr = 0.710237 \pm 0.000016$ (n = 4) and 0.710222 ± 0.000010 (n = 15) for NBS-987 and $^{143}Nd/^{144}Nd = 0.511852 \pm 0.000003$ (n = 5) and 0.511848 ± 0.000004 (n=5) for La Jolla. Sample data are corrected for the offset from the accepted values (0.710250 for NBS-987 and 0.511850 for La Jolla). Total chemistry blanks were <50 pg for Sr and Nd and are considered negligible.

4. RESULTS

4.1. Whole-rock geochemistry and constraints on precursor rocks

Major and trace element compositions of the FTS 9-1 sequence and associated mélange rocks are summarized in Table 1 and Fig. 3. Sample FTS 9-1.6, which is located furthest within the eclogitic part, has slightly elevated SiO_2 contents, and it is suspected that some contamination with the adjacent quartz vein occurred during sample preparation. Therefore, sample FTS 9-1.5A was chosen as representing the least overprinted eclogite of the FTS 9 sequence. Sample FTS 9-1.5A shows a relatively flat chondrite-normalized REE pattern (Fig. 3A) and a N-MORB-normalized trace element pattern with a negative Nb-Ta anomaly, enrichment of U over Th and positive peaks for Sr, Pb, and Li (Fig. 3B). These features are typical for oceanic arc basalts in general and the overall trace element concentrations show significant similarities to a back-arc basin basalt from Vanuatu (Peate et al., 1997). A slight displacement of sample FTS 9-1.5A from the MORB-OIB array to the volcanic arc array in the Th/Yb vs. Nb/Yb diagram (Pearce, 2008) is also consistent with an arc-related basaltic precursor (Fig. 3C). Sample FTS 9-1.1, which represents the most

overprinted blueschist in the FTS 9-1 sequence, is characterized by a small depletion in HREE, a strong depletion in LREE and MREE and correspondingly more pronounced peaks for Sr, Pb, Li and U compared to the eclogite FTS 9-1.5A (Fig. 3A,B). These peaks are partly intensified during the blueschist-facies metasomatic overprint. Since the blueschist formed from the eclogite, its basaltic precursor must have had an affinity to back-arc basin basalts as well. The variety of precursor rocks occurring in the HP/LT belt is illustrated by samples FTS 1-26 and FTS 5-6. The first (FTS 1-26) is an eclogite with a N-MORB-type REE pattern and no negative Nb-Ta anomaly, suggesting N-MORB-like basalt as precursor, although small enrichments of some incompatible elements may indicate a minor arc influence. Relative depletions in Sr and P may be explained by minor metasomatic overprint or preceding igneous fractionation. The second (FTS 5-6) is a blueschist with REE and trace element patterns almost identical to a typical tholeiitic OIB from Hawaii.

For the pillow metabasalts (FTS 4 samples) van der Straaten et al. (2008) showed that the eclogite domains have a basaltic to trachybasaltic composition and normalized REE and trace element patterns similar to tholeiitic OIB. LREE are enriched over HREE and incompatible trace elements are enriched compared to N-MORB. The scatter of FTS 4 eclogites around the tholeiitic OIB on the Th/Yb vs. Nb/Yb diagram confirms the OIB affinity (Fig. 3C).

4.2. Carbon and oxygen isotopes

Carbon and oxygen isotope compositions of carbonate and silicate minerals are presented in Table 2 and Fig. 5. Calcite from the FTS 9-1 sequence shows homogeneous C ($\delta^{13}C$ = -9.4 to -9.0‰) and O ($\delta^{18}O$ = +11.4 to +11.8‰) isotopic compositions. Ankerite from pillow metabasalts and the associated apatite-ankerite vein is considerably heavier and slightly more variable in $\delta^{13}C$ (-1.6 to -2.2‰) and has somewhat higher but very homogenous $\delta^{18}O$ values (+12.8 to +13.3‰). The carbonates of the Tian Shan HP rocks are distinct in their C-O isotope composition from values that are commonly assumed to represent pristine mantle carbon (Fig. 5A). Metamorphic calcite with C-O isotope compositions similar to the FTS 9-1 rocks were found in metabasalts and metasediments in the Catalina Schist (Bebout, 1995). Calcite from various ophiolites (Alps, Corsica) and from metabasalts and calcite veins from the Franciscan overlap with ankerite compositions of the FTS 4 samples.

For the silicates, all minerals from the eclogite-blueschist sequences have $\delta^{18}O$ values that are higher than typical values for mantle-derived rocks based on measurements of olivine and fresh glass (5.3–6.2‰; Eiler et al., 1997; Eiler et al., 2000). The individual mineral O

isotopic compositions overlap with those from eclogite-facies metabasalts from Greece and Ecuador and fall into the range of low-temperature AOC (Fig. 5B). Minerals from the FTS 9-1 sequence have generally lower $\delta^{18}O$ values than the corresponding minerals in the pillow metabasalts.

Mineral-mineral O isotopic equilibria (Fig. 6, Table 2) were evaluated by comparison to equilibrium fractionation calculated based on the modified increment method (Zheng, 1993a,b). For solid solution minerals omphacite, garnet, sodic amphibole and white mica (phengite in FTS 4, paragonite in FTS 9-1), fractionations were calculated for the known composition based on mineral chemical data (van der Straaten et al., 2008; van der Straaten, 2008) assuming linear relationships between the end-member compositions.

In the FTS 9-1 sequence, blueschist-facies glaucophane and paragonite are in O isotopic equilibrium with each other and with garnet and calcite (Fig. 6A). Based on the O isotope fractionation between these four minerals, an average equilibration temperature of 606±22 °C for the blueschist-facies overprint was determined. The paragonite-glaucophane pair was ignored in this calculation because temperatures calculated using this mineral pair are very susceptible to analytical uncertainty due to the very small equilibrium isotopic fractionation (≤0.6‰ at the relevant metamorphic temperatures). Regarding the eclogite-facies assemblage in sample FTS 9-1 (Fig. 6B), the measured phengite-omphacite fractionation (0.32‰) is close to the calculated equilibrium fractionation at 600 °C (0.39‰). The measured O isotope fractionations between omphacite and garnet (0.89‰) and between phengite and garnet (1.21‰) are significantly different from the calculated fractionations (1.58‰ and 1.97‰, respectively, at 600 °C), suggesting that the O isotope composition of garnet re-equilibrated during the blueschist-facies overprint.

For the pillow metabasalts (FTS 4 samples), both equilibrium fractionation and variable displacement from calculated equilibrium values can be observed (Fig. 6C, D). Minerals from samples that contain both eclogite-facies and blueschist-facies domains (samples FTS 4-2.4, 4-3.3 and 4-3.5) tend to show more pronounced deviations from equilibrium. An entirely overprinted blueschist (sample FTS 4-1.1) shows consistent O isotope equilibria between garnet, glaucophane and phengite. The temperature of the blueschist-facies overprint was calculated for sample FTS 4-1.1 based on O isotope fractionation between ankerite, garnet, phengite and glaucophane (Fig. 6C). Note that phengite belongs to the blueschist-facies paragenesis in sample FTS 4-1.1 but paragonite is the blueschist-facies white mica in the sample sequence FTS 9-1. Ignoring the phengite-glaucophane pair, an average temperature of 596±16 °C is obtained. This temperature is in

good agreement with a temperature of 580±10 °C for the retrograde path of phengite-ankerite blueschist determined from phase equilibria (van der Straaten et al., 2008).

4.3. Sr- Nd isotopic data and age determinations

Strontium and Nd isotope data for Tian Shan rocks are listed in Table 3. To evaluate equilibration during metamorphism, the two eclogite-blueschist transition sequences were plotted in Rb-Sr and Sm-Nd isochron diagrams using Isoplot/Ex 3 (Ludwig, 2003; Fig. 7). Blueschist-facies pillow metabasalts (FTS 4 samples) yield a well-defined Rb-Sr isochron (MSWD = 0.97) with an age of 320±11 Ma and an initial $^{87}Sr/^{86}Sr$ ratio of 0.70635±0.00014 (Fig. 7A). The eclogite-facies pillow metabasalts yield a Rb-Sr errorchron (MSWD = 15) with an age of 308±50 Ma and an initial $^{87}Sr/^{86}Sr$ ratio of 0.70629±0.00021 (Fig. 7B), overlapping the respective values of the blueschist-facies samples. All pillow metabasalts samples together give an errorchron (MSWD = 5.8) with an age of 322±11 Ma and an initial $^{87}Sr/^{86}Sr$ of 0.70627±0.00010. In the Sm-Nd isochron diagram (not shown), FTS 4 pillow metabasalts are characterized by a very limited spread in $^{147}Sm/^{144}Nd$, resulting in a poorly defined errorchron age of 330±120 Ma. The initial $^{143}Nd/^{144}Nd$ of the errorchron corresponds to an $\varepsilon Nd_{330\ Ma}$ value of +2.7, similar to the $\varepsilon Nd_{320\ Ma}$ values calculated for the individual blueschist and eclogites samples (Table 3). All these dates seem to have reasonable age significance as they overlap within error with the ~315 Ma age of high-pressure peak metamorphism for the Tian Shan inferred from Lu-Hf garnet growth dating (Klemd et al. 2011) and the successive retrograde reequilibration of white mica around ~311 Ma (Klemd et al., 2005).

Samples from the FTS 9-1 blueschist-eclogite transition did not yield reliable and reasonable Rb-Sr isochron ages because $^{87}Rb/^{86}Sr$ ratios are quite low and span a very limited range. For the Sm-Nd system, an errorchron yielding an age of 600±140 Ma with an initial $^{143}Nd/^{144}Nd$ ratio corresponding to $\varepsilon Nd_{600\ Ma}$ = +7.9 was obtained. Hence, initial $^{87}Sr/^{86}Sr$ ratios and εNd values for the FTS 9-1 sequence were calculated for 600 Ma as well as for 320 Ma to allow for a comparison with the FTS 4 samples (Table 3). It has to be noted that the ~600 Ma "age", possibly representing a crystallization age, is quite uncertain. In particular, the loss of Nd during the metasomatic overprint likely affected the Sm/Nd ratios. All data points for the meta-igneous Tian Shan rocks are displaced from the mantle array towards higher Sr initial isotopic ratios (Fig. 8). The FTS 9-1 blueschists and eclogites fall onto a trend defined by increasing seawater alteration. For t=600 Ma, $^{87}Sr/^{86}Sr$ initial ratios cluster at ~0.707 and εNd values fall into a narrow range from +7.1 to +8.5. Because of the very low $^{87}Rb/^{86}Sr$ ratios, there are no significant differences between the Sr isotopic compositions of

the FTS 9-1 samples calculated at 600 and 320 Ma. The elevated εNd values are similar to a Tian Shan eclogite analyzed by Gao and Klemd (2003) with εNd = +8.9. Considering the isotopic compositions at 320 Ma, FTS 4 pillow metabasalts define a very small field in Sr-Nd isotope space. Initial $^{87}Sr/^{86}Sr$ and εNd vary from 0.7059 to 0.7065 and +2.1 to +2.7, respectively. Other rocks from the Tian Shan mélange show more variability, in particular for $\varepsilon Nd_{320\ Ma}$ (-0.4 to +6.7).

5. DISCUSSION

5.1. Distinction between geochemical changes related to seafloor alteration and blueschist-facies metasomatism

A fluid that was in equilibrium with a rock of a specific composition can adopt the chemical characteristics of the rock in its major and trace element composition. On the other hand, the chemical composition of a rock would shift towards the fluid composition during fluid-rock interaction, and thus the rock would inherit a "fingerprint" of the infiltrating fluid (e.g., Bebout, 1991; Sorensen and Grossman, 1989; Zack and John, 2007). Hence, a comparison of the blueschist-facies, metasomatically altered domains with the less altered eclogitic parts will provide information about the chemical load of the fluid and about fluid source rocks and/or the rocks the fluid equilibrated with.

All of the Tian Shan eclogites and blueschists derive from oceanic basalts. Hence, it has to be evaluated if and to what extent they have been affected by seawater alteration and whether any geochemical signatures of seafloor alteration have been preserved. Pillow basalts are especially susceptible to alteration, since the space between the pillows and associated cooling cracks serves as a fluid pathway and facilitates seawater access. Bebout (2007) used changes in trace element concentrations and trace element ratios involving K, Rb, Ba, Th, Nb and U to distinguish between seawater alteration and mobility during high-pressure metamorphic fluid/rock interaction. Enrichment of K and Rb is a distinct feature of seawater alteration in oceanic basalts (Becker et al., 2000; Staudigel, 2003), whereas Ba is usually not enriched during this process (Bebout, 2007). On the K/Th vs. Ba/Th and Ba/Rb vs. K diagrams (Fig. 9A,B), the FTS 9-1 sequence follows the trends typical for HP/UHP metasomatism and is clearly distinct from seafloor alteration trends. The direction of the trends with increasing degree of blueschist-facies overprint for the FTS 9-1 rocks is similar to the trends from eclogite towards blueschist in the FTS 4 pillow metabasalts. Importantly,

there is a systematic increase in the degree of metasomatic alteration seen in the diagrams with increasing degree of blueschist-facies overprint based on the petrographic observations. It is therefore highly unlikely that the characteristic enrichments of Rb, K and Ba in the blueschist domains of the FTS 9-1 sequence are inherited from seafloor alteration. Instead, the elemental changes with increasing metasomatic overprint for both the FTS 9-1 sequence and the pillow metabasalts are attributed to a HP metasomatic event. Any previous effects of seafloor alteration on the trace element systematics, which may have been present, have been obliterated.

5.2. Characterization of the elemental changes related to metasomatism

Before the metasomatic changes of the blueschist overprint in the FTS 9-1 sequence are discussed in detail, the metasomatic effects in the pillow metabasalts are briefly summarized from van der Straaten et al. (2008). The metasomatic overprint of eclogite pillow metabasalts under blueschist-facies conditions caused an overall volume and mass loss characterized by the loss of Ca, P, Sr, Pb, U, REE and Y due to dissolution and breakdown of apatite, clinozoisite (major reservoir of LREE) and garnet (major reservoir of HREE). In addition, Na, Li and V were lost due to omphacite breakdown during retrogression. Gain of transition metals (Co, Ni, Cu, Zn), Mg, H_2O and CO_2 in the blueschist domains is related to the incorporation of these elements into newly formed glaucophane and ankerite. Formation of blueschist-facies phengite facilitated bulk addition of LILE and H_2O.

In the FTS 9-1 sequence, there is a correlated, successive enrichment of Ba and K from eclogite via mixed eclogite/blueschist domains towards the blueschist (Fig. 9C). LILE are generally assumed to partition into the fluid phase during dehydration processes and reactive fluid flow within AOC and sediments (Kessel et al., 2005; John et al., 2008), in particular if LILE-bearing minerals such as phengite break down and do not recrystallize. Similar enrichments of these fluid-mobile elements were reported from eclogites and blueschists from California (Horodyskyj et al., 2009; Catlos and Sorensen, 2003; Giaramita and Sorensen, 1994). The gain of LILE may be ascribed to a fluid derived from sediments or by reaction with sediments (Horodyskyj et al., 2009; van der Straaten et al., 2008), but intense leaching of AOC may cause similar enrichments in the passing fluids. The FTS 9-1 eclogite-blueschist transition sequence also shows a correlated and systematic gain in the transition metals Co and Ni (Fig. 9D). This enrichment trend points towards the compositions of depleted mantle and orogenic serpentinites. In ultramafic mantle rocks, both Co and Ni are highly enriched relative to mantle-derived basalts because of their compatibility in olivine.

Similar enrichments were observed in retrograde eclogites, which were interpreted to have interacted with serpentinites during exhumation in a subduction channel (e.g., Horodyskyj et al., 2009; van der Straaten et al., 2008).

Evaluating the behavior of the various elements in relation to the mineral phases present provides insight into why certain elements are gained/lost during blueschist-facies overprint in the FTS 9-1 sequence. The addition of LILE can be associated with the formation of paragonite, as white mica is a major host of LILE (e.g., Zack et al., 2001). The gain of CO_2 and P is accommodated by the formation of calcite and apatite, respectively, which both can incorporate Pb and Sr as well (Gao et al., 2007; Spandler et al. 2003). Blueschist-facies glaucophane is able to accommodate Co and Ni (van der Straaten et al., 2008). The loss of MREE and HREE can be attributed to the breakdown of omphacite and garnet. Since apatite is lacking from the FTS 9-1 eclogite, there is no loss of Sr, Pb and P related to apatite breakdown, opposite to what is observed in the pillow metabasalts.

To evaluate the geochemical changes with increasing blueschist overprint in the FTS 9-1 sequence more thoroughly, trace element concentrations are normalized to the composition of eclogite sample FTS 9-1.5A, which represents the least affected rock (Fig. 10A). The systematic increase in LILE and the systematic decrease in Th, U and LREE with increasing metasomatic overprint suggest that the samples analyzed show a real trend related to the metasomatic process as opposed to randomly showing variable elemental enrichments and depletions related to the modal composition. HFSE cluster around a ratio of 1, consistent with relative immobile behavior. Trace element ratios, such as Ba/Th, U/Th and Pb/Ce (Fig. 10B), which are commonly used as tracer for slab fluids in volcanic as well as metasomatized mantle wedge and subducted oceanic crustal rocks (Elliott, 2003; Halama et al., 2009; John et al. 2004; Kessel et al., 2005) show increasing values towards the most overprinted rocks, demonstrating that the relative mobility of these elements is similar to that in subduction-related volcanic systems. The most completely overprinted blueschist (FTS 9-1.1) and eclogite FTS 9-1.5A were then compared in an isocon plot (Fig. 10C) following the procedure of Grant (2005) for a quantitative assessment of elemental changes. Gains and losses of individual elements during the metasomatism were calculated by assuming a reference frame of immobile elements that are neither added nor lost. Following Grant (2005), the isocon is based on the slope C_i^A/C_i^O (C_i^A and C_i^O are the concentrations of species “i" in the altered and in the original rock, respectively), so that scaling is irrelevant to the slope and can simply be used to improve visualization. In Fig. 10C, the data are first sorted on C_i^O into two groups, oxides and trace elements, and then scaled to even values in decreasing concentrations, except

for H_2O and K_2O that are scaled to low values because of the drastic changes (see supplementary data). As immobile species, TiO_2, P_2O_5, Zr, Hf, Nb and Ta were chosen. These elements fulfill two important criteria that justify their choice as immobile species. First, the individual slopes in the isocon diagram to the respective data points of these elements cluster near 1. Slopes near 1 are expected for immobile elements if the overall mass change of the system were small. Second, these elements are known to usually behave in an immobile manner in many different environments. Taken together, the average slope for these 6 elements is 1.0149, indicating a very small mass loss of the total system causing a small passive enrichment of the immobile species. Compared to the eclogite, the blueschist domain of the FTS 9-1 sequence has gained volatiles (CO_2, H_2O), LILE (Cs, Ba, Rb, K), Sr, Pb, Mg and some transition metals (Ni, Co, Zn), whereas REE, in particular LREE, Ca, U, Th and other transition metals (V, Sc, Cu) were lost (Fig. 10C). The highest elemental gains are observed for K, Rb and Ba (~250% relative to FTS 9-1.5A) and the volatiles. Cobalt and Ni show relative gains of ~50%. The most significant mass loss of up to ~90% is observed for the LREE.

Besides the gain in Ni and Co, contemporaneous gain of Mg and loss of Ca and REE also point to a metasomatic fluid that equilibrated with a rock of peridotitic composition prior to infiltration. As for the FTS 4 pillow metabasalts, which show similar enrichment-depletion trends (van der Straaten et al., 2008), the infiltrating fluid likely interacted with mantle wedge peridotite or the subducted peridotite of the slab. For the enrichment in LILE, however, it is not possible to distinguish between interaction of the fluid with sediments or leaching from AOC. The gain of CO_2 and the formation of calcite in the FTS 9-1 blueschists can be related to CO_2 derived from subducted carbonate-rich sediments or from carbonates precipitated by hydrothermal activity in AOC or serpentinized slab mantle (Schroeder et al., 2002; Da Costa et al., 2008; Eickmann et al., 2009). Carbonates are usually quite stable at HP conditions in subduction zones (Molina and Poli, 2000), but during open-system fluid flow, CO_2 stored in secondary carbonates in metamorphosed mafic oceanic rocks can be released during prograde metamorphism. For instance, the transformation of carbonate-bearing blueschists into prograde eclogites (in the Tian Shan as well) due to high fluid fluxes at open-system conditions caused the release of up to 95% CO_2 (John et al., 2008). More information on the source of CO_2 may be gained from C-O isotope data.

5.3. Stable isotope constraints on nature and role of fluids

Stable isotope studies in metamorphic rocks can provide information about rock protoliths, if a primary signal is preserved, and about processes affecting the rock during its metamorphic history. For metamorphosed carbonates, the processes of Rayleigh devolatilization and infiltration of external fluids were recognized using C- and O-isotopic systematics (Nabelek et al., 1984; Bebout and Carlson, 1986). However, the identification of fluid sources is complicated because of the large variations in C-O isotopic compositions for disseminated and vein carbonate from metamorphic rocks (Fig. 5A). In case of the Tian Shan samples investigated here, carbonates were added during the blueschist-facies overprint and are related to a fluid infiltration event. An origin as residual carbonate, as proposed for carbonates in eclogites from Norway (Agrinier et al., 1985), is therefore unlikely. A significant contribution of mantle C can be excluded based on the distinct $\delta^{13}C$ values and the relatively low C contents in the mantle. Ankerite from FTS 4 samples with $\delta^{13}C$ of about -2‰ has a sedimentary inorganic carbon signature because of the overlap in $\delta^{13}C$ with unaltered marine limestones ($\delta^{13}C$ = -2 to +4; Sharp, 2007). Carbonates from ophiolites, ranging from -4 to +3‰ in $\delta^{13}C$, were also interpreted to reflect a marine C isotope signal, either by derivation from calcareous metasediments (Cartwright and Barnicoat, 1999) or inherited from early seafloor alteration (Miller et al., 2001). The $\delta^{13}C$ signature of the carbonates that represent the C source of the fluid may have been slightly modified by metamorphism, because devolatilization produces a moderate decrease in $\delta^{13}C$ and a significant decrease in $\delta^{18}O$ in the residue due to the release of high-$\delta^{18}O$ CO_2 by decarbonation reactions (Agrinier et al., 1985). Hence, an ultimately marine sedimentary source for C in the vein-forming fluid that formed the apatite-ankerite vein and the associated disseminated ankerite in the pillow metabasalts is indicated. For the origin of the low $\delta^{13}C$ values of calcite in the FTS 9-1 blueschists ($\delta^{13}C$ = -9.1±0.2‰), two scenarios will be evaluated: 1) Mobilization of C from previously devolatilized sedimentary inorganic carbonate with an initial $\delta^{13}C$ of 0‰ and 2) a contribution of organic carbon. In the first case, >90% of devolatilization is required to reduce $\delta^{13}C$ from an original value of 0‰ to values < -9‰ if a temperature of 600°C and an accordant CO_2-calcite fractionation factor α = 1.00372 (Scheele and Hoefs, 1992) are assumed. This scenario appears unlikely because it is difficult to explain why the first 90% of devolatilized CO_2, constituting the bulk of available C, should not have precipitated in the blueschist as carbonate with $\delta^{13}C$ values between -9 and 0‰. Hence, a contribution of CO_2 to the metamorphic fluid from oxidation of organic C is considered more likely. Organic C has been detected in eclogites, where $\delta^{13}C$ values as low as -26‰ were interpreted to reflect the

isotopic composition of C in the eclogite precursors (Zheng et al., 2000). Relatively light $\delta^{13}C$ values (-13 to -6‰) of calcite veins in the Catalina Schist, similar to those of the FTS 9-1 calcite, were also interpreted to have formed from fluids that equilibrated with carbonaceous matter of organic origin (Bebout and Barton, 1993). For FTS 9-1 calcite, the origin of C is therefore attributed to a mixture of organic C and inorganic marine sedimentary/hydrothermal C, mobilized during subduction and later reprecipitated during the blueschist-facies overprint. Based on mobilization and transport of C in subduction zones (Beinlich et al., 2010; Gao et al., 2007; John et al., 2008;), its subsequent sequestration in HP metamorphic rocks as seen in this study demonstrates that subducted C may not entirely be transported into the deep mantle beyond subarc regions, but can be transported back towards the Earth's surface in the subduction channel.

Based on the O isotopic compositions of constituent minerals, whole rock $\delta^{18}O$ values of the Tian Shan eclogites and blueschists can be estimated to range between 8 and 10‰. These $\delta^{18}O$ values are significantly higher than those of mantle-derived basaltic rocks (5.2-6.3‰; Eiler et al., 1997; Eiler et al., 2000). This observation cannot be explained by dehydration, because common dehydration reactions lead to decreasing $\delta^{18}O$ values in the residual rock. Moreover, the fraction of O remaining in the rock is relatively large (> 0.9), so such reactions cannot change $\delta^{18}O$ values by more than a few per mil (Sharp, 2007). Therefore, elevated $\delta^{18}O$ values may be related to inherited effects of low-temperature seawater alteration from the precursor rock, or to the metasomatic fluid itself (Putlitz et al., 2000; Halama et al., 2011). Both possibilities will be discussed in turn.

It is well established that seawater alteration of basaltic rocks on the ocean floor increases the $\delta^{18}O$ values at low temperatures (<150°C) (Gregory and Taylor, 1981). At greater depth and higher temperatures (100-400°C), $\delta^{18}O$ values decrease to values lower than that of the typical mantle composition (Mühlenbachs and Clayton, 1976; Gregory and Taylor 1981). Due to higher whole rock $\delta^{18}O$ values (11-14‰) in HP rocks compared to fresh MORB, an oxygen isotope signature indicative of seawater alteration was proposed for several occurrences of subduction-related metamorphic rocks (Miller et al., 1988; Putlitz et al., 2000; Halama et al., 2011). In the Tian Shan samples, there are two features that point towards a pre-subduction seafloor alteration. First, preserved inter-mineral O isotope disequilibria in samples containing eclogite remnants suggest incomplete equilibration with metasomatic fluids (Fig. 6B, D), but none of the minerals analyzed has $\delta^{18}O$ values within the range for fresh oceanic basalts. Instead, they fall into the range observed for low-T AOC. Second, garnet in transitional eclogite-blueschist samples FTS 4-2.4 and FTS 4-3.5 is higher

in $\delta^{18}O$ than garnet from the most overprinted and well-equilibrated blueschist sample FTS 4-1.1, suggesting that these samples had even higher $\delta^{18}O$ inherited from seafloor alteration before the retrograde metasomatic overprint.

Elevated $\delta^{18}O$ values can also result from fluid-rock interaction during burial and metamorphism (Chamberlain and Conrad, 1991). The O isotope composition of the fluid that equilibrated with blueschist sample FTS 4-1.1 can be estimated using known fractionation factors between minerals and water for 600°C (Zheng, 1993a,b). The four minerals analyzed yield very homogenous $\delta^{18}O_{fluid}$ values with an average of ~11.2‰. If the same calculation is performed for those minerals that yield a well-defined O isotope temperature in sample FTS 9-1 (garnet, glaucophane and paragonite), a $\delta^{18}O_{fluid}$ value of ~10.2‰ is obtained. Regarding the inventory of subducted material that may have acted as a potential fluid source, oceanic sediments are isotopically heavier ($\delta^{18}O$ = +11.5 to +28.5‰; Savin and Epstein, 1970), whereas serpentinized peridotites are lighter ($\delta^{18}O$ = +1.2 to +8.1‰; Cartwright and Barnicoat, 1999; Frueh-Green et al., 2001; Miller et al., 2001). The best overlap between potential subducted material and calculated fluid compositions occurs for pillow lavas and metabasalts as observed in ophiolites from the Alps and Corsica ($\delta^{18}O$ = +4.4 to +15.6‰; Cartwright and Barnicoat, 1999; Miller et al., 2001). Clearly, the devolatilization of subducted oceanic crust and mantle can yield a wide range in O isotopic compositions of the released fluids. The Tian Shan O isotope data suggest that on the one hand, the HP rocks have inherited a seafoor alteration signal, preserved in the eclogites. On the other hand, the blueschist-facies rocks indicate that fluids derived from dehydrating high-pressure equivalents of AOC played a major role in the retrograde overprint of the investigated samples, although small contributions from ultramafic or sedimentary sources cannot be excluded. This interpretation is supported by increasing Ba/Th ratios with increasing metasomatic overprint (Fig. 10B) because elevated Ba/Th ratios can be attributed to a fluid component from mafic AOC (Elliott, 2003).

5.4. Constraints from Sr-Nd isotopes on seafloor alteration and the source of the metasomatizing fluid

Combined Sr and Nd isotope ratios are a sensitive indicator of seawater alteration in oceanic basalts and peridotites because Sr isotopic ratios are increased, whereas Nd isotopes are not significantly affected (McCulloch et al., 1980; Staudigel et al., 1995; Hoernle, 1998; Staudigel, 2003). For the eclogites and blueschists from the Tian Shan, εNd values are

consistent with the interpretations of precursors based on trace element signatures. The positive εNd values of the FTS 9-1 sequence and of eclogite sample FTS 1-26 overlap with depleted mantle values and are consistent with back-arc basin basalt and N-MORB, respectively, as precursor. Moderately positive εNd values agree well with the OIB trace element signature of the FTS 4 pillow metabasalts. In contrast, Sr isotopic ratios are displaced from the mantle array and shifted to high (≥ 0.706) values (Fig. 8). This shift may be explained by an unusual precursor composition, by alteration on the ocean floor or by influx of a metasomatic fluid. These three possibilities will be discussed in turn.

To test whether the Tian Shan eclogites just reflect an unusual precursor Sr-Nd isotope composition, they are compared to OIBs that are characterized by radiogenic Sr isotope signatures (Fig. 8). FTS 9-1 samples and eclogite FTS 1-26 have εNd values that are several ε-units higher than basaltic lavas from Samoa, which are interpreted to contain a recycled crustal component (Jackson et al., 2007). Since these Tian Shan samples plot far away from any unaltered oceanic basalt composition, they cannot purely reflect the composition of their magmatic precursor rocks. The εNd values of the FTS 4 pillow metabasalts and blueschist FTS 5-6 are similar to OIB from the Kerguelen, but the data are displaced towards higher $^{87}Sr/^{86}Sr$ ratios in the Sr-Nd isotope diagram, suggesting a trend similar to alteration of oceanic crust. Although these Tian Shan samples overlap with Samoan OIB, several trace element features that are typical for the Samoan basalts, such as negative Ti, Eu, Sr and Nb-Ta anomalies and positive Zr-Hf anomalies, are absent or only of minor significance. In summary, it can be concluded that the Tian Shan samples do not solely reflect their protolith composition, but have been affected by varying degrees of seafloor alteration and/or metasomatic overprint.

The well-defined Rb-Sr isochron age of 320±11 Ma with an initial Sr isotope ratio of 0.70635±0.00014 for the FTS 4 blueschist-facies pillow metabasalts (Fig. 7A) suggests that Sr isotopes have re-equilibrated during the blueschist-facies overprint, in agreement with the geochemical evidence for HP/UHP metasomatism. Similar ages and initial ratios obtained from the eclogitic parts of the metabasalts only (Fig. 7B) also suggest Sr isotope homogenization. Homogenization of Sr isotopes by HP fluid-rock interaction was previously recognized for eclogite- and amphibolite facies fluid infiltration events and used to date HP fluid-rock interaction (Glodny et al., 2003, 2008). The existence of the FTS 4 isochron strongly points to a metasomatic fluid infiltration event that caused resetting of the isotopic system in the Tian Shan pillow metabasalts because of two reasons: First, from seawater alteration alone a wide range of initial Sr isotope compositions would be expected, as

observed for seawater-altered eclogites (e.g., Miller et al., 1988; Halama et al., 2011). Second, it is highly unlikely that if seawater alteration had homogenized Sr isotopes, the resulting isochron age would be similar to the time of HP metamorphism. Instead, the age of ~320 Ma, which is in good agreement with the age of the high-pressure metamorphism of ~315 Ma (Klemd et al., 2011), overlaps within error the age range for a blueschist-facies, post-peak metamorphic stage during exhumation (323-303 Ma), which was determined using K-Ar, ^{40}Ar-^{39}Ar and Rb-Sr white mica chronology (Klemd et al., 2005). Sr isotopic ratios of the FTS 9-1 sequence, corrected to 320 Ma, cluster tightly (^{87}Sr/^{86}Sr ~ 0.7071), indicating isotopic equilibration. Maximum ^{87}Sr/^{86}Sr values of the precursor seawater-altered crust and of a fluid derived from altered oceanic lithosphere can be estimated from the Sr isotopic composition of seawater during Ordovician to Carboniferous times (0.7075-0.709; Veizer, 1989), i.e. during the time the protoliths formed and subduction started. All FTS 9-1 metabasalts have initial Sr isotope ratios that are lower than these values and hence consistent with both, seawater alteration and infiltration of fluid derived from dehydrating seawater-altered oceanic lithosphere (SAOL). The term SAOL is used here to combine altered crust and altered/serpentinized mantle and to simultaneously separate the sediments from the lithospheric portion of the slab.

Fluid-rock interaction in Sr-Nd isotope space is modeled based on the assumption that the metabasalts reflect the Nd isotope composition of their precursor (Fig. 11). Model parameters are listed in Table 4. Mixing of FTS 4 precursor basalt with two end-member sediment-derived fluids shows a rapid change in the infiltrated rocks to lower εNd values. A significant sedimentary input to the metasomatic fluid that equilibrated with the pillow metabasalts is therefore not permitted. In contrast, the mixing trend with fluid derived from SAOL goes right through the FTS 4 data points. The choice of the SAOL end-member composition is based on the observation that intensely altered peridotites reflect the Sr-Nd characteristics of seawater (Snow and Reisberg, 1995). A distinction between altered peridotites and altered basalts as the dominant fluid source is not possible on the basis of Sr-Nd data. Due to the low Nd contents and the relative preference of Nd for the rock (Table 4), fluids derived from SAOL will always have little effect on εNd values of the basalt, independent of whether the SAOL source has completely inherited the seawater Sr-Nd signature (as modeled) or not. Slab fluids, assumed to consist of 80% SAOL-derived fluid and 20% sediment-derived fluid, largely inherit the Nd isotope signature of the sediment. Even if a positive εNd value is assumed for the SAOL-fluid, the slab fluid's εNd will not deviate significantly from the sediment value. For the proportions of sediment and SAOL in the slab

fluid, even a change of 10 εNd units for the SAOL-fluid would not change εNd of the slab fluid by more than 1 εNd unit. This allows an estimate of how much sediment-derived fluid was incorporated into the slab fluid that caused the retrograde overprint in the pillow metabasalts. One can conclude that the sediment fluid addition was less than 20%, and that the metasomatic fluid was predominantly derived from altered oceanic lithosphere, supported by alteration trends seen in oceanic crust and oceanic peridotites (Figs. 8 and 11). A simplification of the model is that it does not consider loss of Nd during HP metamorphism, which occurs in both, the FTS 9-1 sequence and the FTS 4 pillow metabasalts. However, since Nd loss would only increase the susceptibility of the eclogite εNd values to modification, one can conclude that sediment-derived fluid addition to the mixed fluid was likely significantly less than 20%. Thus modeling strongly suggests that overprinting of the FTS 9-1 sequence was also largely derived from seawater-altered oceanic lithosphere with little influence from sedimentary fluid sources.

6. SUMMARY AND CONCLUSIONS

Oceanic basalts from the Tian Shan HP/LT metamorphic belt show laterally (dm to m scale) a retrograde, blueschist-facies overprint of pre-existing eclogite-facies rocks. Two eclogite-blueschist transitions, which were investigated in detail, show elemental enrichment trends that are typical for HP/UHP metasomatism with increasing degree of blueschist-facies overprint. In both sequences, loss of Ca, V, U and REE and enrichment of LILE, volatiles, Mg and some transition metals, such as Co and Ni, are observed in the blueschist-facies parts relative to the preserved eclogitic parts. The coupled enrichments of Co and Ni point to fluid interaction with ultramafic mantle rocks, consistent with the assumed exhumation in a subduction channel. Addition of LILE suggests a sedimentary contribution, although leaching of altered oceanic crust and mantle rocks may have similar effects. C-O-Sr-Nd isotopic data, which were obtained to constrain protolith composition and to distinguish between the effects of seafloor alteration and HP metasomatism, result in the following conclusions:

1. Carbon isotopes in carbonates formed in the blueschist-facies parts indicate a contribution of organic C for the FTS 9-1 sequence and show an inorganic sedimentary/hydrothermal carbonate signature for the pillow metabasalts. The latter overlap in their C-O isotope signature with ophiolites and various metabasalts, suggesting that C was probably stored in altered oceanic crust because marine carbonates typically have higher $\delta^{18}O$

values. The contribution of organic C shows that an integrative signal of mixed organic and inorganic C sources can be precipitated in carbonates during HP metasomatism. This indicates that CO_2 can be mobilized during subduction and that it can remain sequestered in the subduction zone without being transported deeper into the mantle or expelled in the volcanic arc.

2. Oxygen isotope compositions of silicate minerals are heavier than typical mantle values, and the overlap with low-T altered oceanic crust suggests inheritance of a seawater alteration signal. Oxygen isotopic equilibrium from eclogite-facies conditions is only partly preserved (omphacite-phengite in FTS 9-1). During the blueschist-facies overprint, equilibrium has been attained between glaucophane, white mica (FTS 9-1: paragonite; pillow metabasalts: phengite), garnet and carbonates, yielding equilibration temperatures of 580-630 °C. Estimates of $\delta^{18}O$ for the metasomatic fluids that equilibrated at blueschist-facies conditions range from +10.2‰ to +11.2‰, for which the best overlap with possible source rocks exists for pillow lavas and metabasalts from ophiolites, further pointing to the influence of altered oceanic crust in the generation of the fluids.

3. A Rb-Sr isochron for the FTS 4 pillow metabasalts yields an age of 320±11 Ma, consistent with previous determinations for the age of metamorphism. This indicates full isotopic equilibration during the blueschist-facies metasomatic event. Modeling alteration of a hypothetical basaltic protolith, originally plotting on the mantle array, with various potential fluids indicates that the fluid that metasomatized the pillow metabasalts is largely derived from seawater-altered oceanic lithosphere with a sedimentary contribution of less than 20%.

In summary, the metasomatized rocks provide evidence for reactive fluid flow through the oceanic slab during exhumation at the slab-wedge interface (Fig. 12). The metamorphic fluids infiltrating the eclogites were predominantly derived from mafic and ultramafic rocks of the seawater-altered oceanic lithosphere with smaller contributions from metasediments. Thus, the fluid interacted with various lithologies that all contributed to the observed elemental and isotopic changes (Fig. 12). Individual isotope systems often yield equivocal results for the potential fluid source. The combination of several isotopic systems, coupled with a good characterization of the rocks in terms of major and trace element geochemistry, is required to disentangle the effects of protolith heterogeneity and various fluid source components. This integrated approach allows the complexity of fluid flow and associated metasomatic changes in subduction zones to be fully appreciated.

7. ACKNOWLEDGEMENTS

J. Gao is thanked for the support and management of the fieldwork in the Tian Shan. We also like to thank A. Pack and R. Przybilla (University of Göttingen) for oxygen isotope analyses. The help of D. Garbe-Schönberg and U. Westernströer (University of Kiel) with ICP-MS analyses is greatly appreciated. Constructive comments by R. Rudnick, H. Marschall and an anonymous reviewer on an earlier version of this manuscript helped to clarify our argumentation. Two detailed reviews by S. Penniston-Dorland and an anonymous reviewer and the editorial comments by L. Reisberg significantly improved the manuscript and are highly appreciated. The Deutsche Forschungsgemeinschaft supported this study by grant Sche 265/S1-2. This publication is contribution no. 161 of the Sonderforschungsbereich 574 "Volatiles and Fluids in Subduction Zones" at Kiel University.

References

Agrinier, P., Javoy, M., Smith, D.C. and Pineau, F., 1985. Carbon and oxygen isotopes in eclogites, amphibolites, veins and marbles from the Western Gneiss Region, Norway. Chem. Geol., 52, 145-162.

Alt, J.C., Laverne, C. and Muehlenbachs, K., 1985. Alteration of the upper oceanic crust: mineralogy and processes in Deep Sea Drilling Project hole 504B, leg 83. Deep Sea Drilling Project Initial Reports, 83, 217-248.

Austrheim, H., 1987. Eclogitization of lower crustal granulites by fluid migration through shear zones. Earth Planet. Sci. Lett., 81, 221-232.

Baker, J., Matthews, A., Mattey, D., Rowley, D. and Xue, F., 1997. Fluid-rock interactions during ultra-high pressure metamorphism, Dabie Shan, China. Geochim. Cosmochim. Acta, 61, 1685-1696.

Bebout, G.E., 1991. Field-based evidence for devolatilization in subduction zones: Implications for arc magmatism. Science, 251, 413-416.

Bebout, G.E., 1995. The impact of subduction-zone metamorphism on mantle-ocean chemical cycling. Chem. Geol., 126, 191-218.

Bebout, G.E., 2007. Metamorphic chemical geodynamics of subduction zones. Earth Planet. Sci. Lett., 260, 373-393.

Bebout, G.E. and Barton, M.D., 1989. Fluid flow and metasomatism in a subduction zone hydrothermal system: Catalina Schist terrane, California. Geology, 17, 976-980.

Bebout, G.E. and Barton, M.D., 1993. Metasomatism during subduction: products and possible paths in the Catalina Schist, California. Chem. Geol., 180, 61-92.

Bebout, G.E. and Carlson, W.D., 1986. Fluid evolution and transport during metamorphism: evidence from the Llano Uplift, Texas. Contrib. Mineral. Petrol., 92, 518-529.

Becker, H., Jochum, K.P. and Carlson, R.W., 2000. Trace element fractionation during dehydration of eclogites from high-pressure terranes and the implications for element fluxes in subduction zones. Chem. Geol., 163, 65-99.

Beinlich, A., Klemd, R., John, T. and Gao, J., 2010. Trace-element mobilization during Ca-metasomatism along a major fluid conduit: Eclogitization of a blueschist as a consequence of fluid-rock interaction. Geochim. Cosmochim. Acta, 74, 1892-1922.

Boynton, W.V., 1984. Geochemistry of the rare earth elements: meteorite studies. In: P. Henderson (Editor), Rare Earth Element Geochemistry. Elsevier, Amsterdam, pp. 63-114.

Breeding, C.M., Ague, J.J. and Bröcker, M., 2004. Fluid-metasedimentary rock interactions in subduction-zone mélange: Implications for the chemical composition of arc magmas. Geology, 32, 1041-1044.

Cartwright, I. and Barnicoat, A.C., 1999. Stable isotope geochemistry of Alpine ophiolites: a window to ocean-floor hydrothermal alteration and constraints on fluid-rock interaction during high-pressure metamorphism. Int. J. Earth Sci., 88, 219-235.

Catlos, E.J. and Sorensen, S.S., 2003. Phengite-based chronology of K- and Ba-rich fluid flow in two paleosubduction zones. Science, 299, 92-95.

Chamberlain, C.P. and Conrad, M.E., 1991. Oxygen isotope zoning in garnet. Science, 254, 403-406.

Cloos, M. and Shreve, R.L., 1988. Subduction-channel model of prism accretion, melange formation, sediment subduction, and subduction erosion at convergent plate margins; Part I, Background and description. Pure Appl. Geophys., 128, 455-500.

Cocker, J.D., Griffin, B.J. and Muehlenbachs, K., 1982. Oxygen and carbon isotope evidence for seawater-hydrothermal alteration of the Macquarie Island ophiolite. Earth Planet. Sci. Lett., 61, 112-122.

Da Costa, I.R., Barriga, F.J.A.S. and Taylor, R.N., 2008. Late seafloor carbonate precipitation in serpentinites from the Rainbow and Saldanha sites (Mid-Atlantic Ridge). Eur. J. Mineral., 20, 173-181.

Des Marais, D.J. and Moore, J.G., 1984. Carbon and its isotopes in mid-oceanic basaltic glasses. Earth Planet. Sci. Lett., 69, 43-57.

Eickmann, B., Bach, W. and Peckmann, J., 2009. Authigenesis of carbonate minerals in modern and Devonian ocean-floor hard rocks. J. Geol., 117, 307-323.

Eiler, J.M. et al., 1997. Oxygen isotope variations in ocean island basalt phenocrysts. Geochim. Cosmochim. Acta, 61, 2281-2293.

Eiler, J.M., Schiano, P., Kitchen, N. and Stolper, E.M., 2000. Oxygen-isotope evidence for recycled crust in the sources of mid-ocean-ridge basalts. Nature, 403, 530-534.

Elliott, T., 2003. Tracers of the slab. In: J. Eiler (Editor), Inside the Subduction Factory, American Geophysical Union, Washington DC, pp. 23-45.

Früh-Green, G., Scambelluri, M. and Vallis, F., 2001. O-H isotope ratios of high-pressure ultramafic rocks: Implications for fluid sources and mobility in the subducted hydrous mantle. Contrib. Mineral. Petrol., 141, 145-159.

Gao, J. and Klemd, R., 2001. Primary fluids entrapped at blueschist to eclogite transition: evidence from the Tianshan meta-subduction complex in northwest China. Contrib. Mineral. Petrol., 142, 1-14.

Gao, J. and Klemd, R., 2003. Formation of HP-LT rocks and their tectonic implications in the western Tianshan Orogen, NW China; geochemical and age constraints. Lithos, 66, 1-22.

Gao, J. et al., 1995. The mineralogy, petrology, metamorphic PTDt trajectory and exhumation mechanism of blueschists, south Tian Shan, northwestern China. Tectonophysics, 250, 151-168.

Gao, J., John, T., Klemd, R. and Xiong, X., 2007. Mobilization of Ti-Nb-Ta during subduction: evidence from rutile-bearing dehydration segregations and veins hosted in eclogite, Tianshan, NW China. Geochim. Cosmochim. Acta, 71, 4974-4996.

Gao, J., Klemd, R., Zhang, L., Wang, Z. and Xiao, X., 1999. P-T path of high-pressure/low-temperature rocks and tectonic implications in the western Tian Shan mountains, NW China. J. met. Geol., 17, 621-636.

Gao, J., Li, M., He, G. and Xiao, X., 1998. Paleozoic tectonic evolution of the Tianshan Orogen, northwestern China. Tectonophysics, 287, 213-231.

Garbe-Schönberg, C.D., 1993. Simultaneous determination of 37 trace elements in 28 international rock standards by ICP-MS. Geostandard Newsletter, 17, 81-97.

Gerya, T.V., Stöckhert, B. and Perchuk, A.L., 2002. Exhumation of high-pressure metamorphic rocks in a subduction channel: A numerical simulation. Tectonics, 21(6), 1056, doi:10.1029/2002TC001406.

Giaramita, M.J. and Sorensen, S.S., 1994. Primary fluids in low-temperature eclogites: evidence from two subduction complexes (Dominican Republic, and California, USA). Contrib. Mineral. Petrol., 117, 279-292.

Glodny, J., Austrheim, H., Molina, J.F., Rusin, A. and Seward, D., 2003. Rb/Sr record of fluid-rock interaction in eclogites: The Marun-Keu complex, Polar Urals, Russia. Geochim. Cosmochim. Acta, 67, 4353-4371.

Glodny, J., Kühn, A. and Austrheim, H., 2008. Geochronology of fluid-induced eclogite and amphibolite facies metamorphic reactions in a subduction-collision system, Bergen Arcs, Norway. Contrib. Mineral. Petrol., 156, 27-48.

Goldstein, S.L., O'Nions, R.K. and Hamilton, P.J., 1984. A Sm-Nd study of atmospheric dusts and particulates from major river systems. Earth Planet. Sci. Lett., 70, 221-236.

Grant, J.A., 2005. Isocon analysis: A brief review of the method and applications. Phys. Chem. Earth, 30, 997-1004.

Gregory, R.T. and Taylor, H.P., 1981. An oxygen isotope profile in a section of Cretaceous oceanic crust, Samail ophiolite, Oman: Evidence for $\delta^{18}O$ buffering of the oceans by deep (> 5 km) seawater-hydrothermal circulation at mid-ocean ridges. J. Geophys. Res., 86 (B4), 2737-2755.

Halama , R., Bebout, G.E., John, T. and Schenk, V., 2010. Nitrogen recycling in subducted oceanic lithosphere: The record in high- and ultrahigh-pressure metabasaltic rocks. Geochim. Cosmochim. Acta, 74, 1636-1652.

Halama, R., John, T., Herms, P., Hauff, F. and Schenk, V., 2011. A stable (Li, O) and radiogenic (Sr, Nd) isotope perspective on metasomatic processes in a subducting slab. Chem. Geol., 281, 151-166.

Halama, R., Savov, I.P., Rudnick, R.L., McDonough, W.F., 2009. Insights into Li and Li isotope cycling and sub-arc metasomatism from veined mantle xenoliths, Kamchatka. Contrib. Mineral. Petrol. 158, 197-222.

Hattori, K. and Guillot, S., 2003. Volcanic fronts form as a consequence of serpentinite dehydration in the forearc mantle wedge. Geology, 31, 525-528.

Hawkesworth, C.J., Gallagher, K., Hergt, J.M. and McDermott, F., 1993. Mantle and slab contributions in arc magmas. Ann. Rev. Earth Planet. Sci., 21, 175-204.

Hermann, J., 2002. Allanite: thorium and light rare earth element carrier in subducted crust. Chem. Geol., 192, 289-306.

Hermann, J., Spandler, C., Hack, A. and Korsakov, A.V., 2006. Aqueous fluids and hydrous melts in high-pressure and ultra-high pressure rocks: Implications for element transfer in subduction zones. Lithos, 92, 399-417.

Hoernle, K., 1998. Geochemistry of Jurassic Oceanic Crust beneath Gran Canaria (Canary Islands): Implications for crustal recycling and assimilation. J. Petrol., 39, 859-880.

Hoernle, K.A. and Tilton, G.R., 1991. Sr-Nd-Pb isotope data for Fuerteventura (Canary Islands) basal complex and subaerial volcanics: applications to magma genesis and evolution. Schweizerische Mineralogische und Petrographische Mitteilungen, 71, 3-18.

Horodyskyj, U., Lee, C.-T.A. and Luffi, P., 2009. Geochemical evidence for exhumation of eclogite via serpentinite channels in ocean-continent subduction zones. Geosphere, 5, 426-438.

Hyndman, R.D. and Peacock, S.M., 2003. Serpentinization of the forearc mantle. Earth Planet. Sci. Lett., 212, 417-432.

Jackson, M.G. et al., 2007. The return of subducted continental crust in Samoan lavas. Nature, 448, 684-687.

John, T., Klemd, R., Gao, J. and Garbe-Schönberg, C.D., 2008. Trace-element mobilization in slabs due to non steady-state fluid-rock interaction: constraints from an eclogite-facies transport vein in blueschist (Tianshan, China). Lithos, 103, 1-24.

John, T., Scambelluri, M., Frische, M., Barnes, J.D. & Bach, W. (2011). Dehydration of subducting serpentinite: implications for halogen mobility in subduction zones and the deep halogen cycle. Earth and Planetary Science Letters, 308, 65-76.

John, T., Scherer, E., Haase, K.M. and Schenk, V., 2004. Trace element fractionation during fluid-induced eclogitization in a subducting slab: trace element and Lu-Hf/Sm-Nd isotope systematics. Earth Planet. Sci. Lett., 227, 441-456.

Kelemen, P.B., Hanghøj, K. and Greene, A.R., 2003. One view of the Geochemistry of subduction-related magmatic arcs, with an emphasis on primitive andesite and lower crust. In: R.L. Rudnick (Editor), Treatise on Geochemistry, volume 3, The Crust. Treatise on Geochemistry, pp. 593-659.

Kelley, K.A., Plank, T., Ludden, J. and Staudigel, H., 2003. Composition of altered oceanic crust at ODP sites 801 and 1149. Geochem. Geophys. Geosyst., 4, 8910, doi:10.1029/2002GC000435.

Kessel, R., Schmidt, M.W., Ulmer, P. and Pettke, T., 2005. Trace element signature of subduction-zone fluids, melts and supercritical liquids at 120-180 km depth. Nature, 437, 724-727.

King, R.L., Bebout, G.E., Moriguti, T. and Nakamura, E., 2006. Elemental mixing systematics and Sr-Nd isotope geochemistry of mélange formation: Obstacles to identification of fluid sources to arc volcanics. Earth Planet. Sci. Lett., 246, 288-304.

Klemd, R. et al., 2005. New age constraints on the metamorphic evolution of the high-pressure/low-temperature belt in the western Tianshan mountains, NW China. J. Geol., 113, 157-168.

Klemd, R., Schröter, F.C., Will, T.M. and Gao, J., 2002. P-T evolution of glaucophane-omphacite bearing HP-LT rocks in the western Tianshan Orogen, NW China; new evidence for Alpine-type tectonics. J. met. Geol., 20, 239-254.

Klemd, R., John, T., Scherer, E.E., Rondenay, S. & Gao, J. (2011). Change in dip of subducting slabs at greater depths: petrological and geochronological evidence from HP-UHP rocks (Tianshan, NW-China). Earth and Planetary Science Letters, 310, 9-20.

Kyser, T.K., O'Neil, J.R. and Carmichael, I.S.E., 1982. Genetic relations among basic lavas and ultramafic nodules: Evidence from oxygen isotope compositions. Contrib. Mineral. Petrol., 81, 88-102.

Ludwig, K.R., 2003. Isoplot/Ex version 3. A geochronological toolkit for Microsoft Excel. Berkeley Geochronology Center, Special Publication, 4, 1-71.

Lü, Z., Zhang, L., Du, J. and Bucher, K., 2008. Coesite inclusions in garnet from eclogitic rocks in western Tianshan, northwest China: Convincing proof of UHP metamorphism. American Mineralogist, 93, 1845-1850.

Lü, Z., Zhang, L., Du, J. and Bucher, K., 2009. Petrology of coesite-bearing eclogite from Habutengsu Valley, western Tianshan, NW China and its tectonometamorphic implication. J. met. Geol., 27, 773-787.

Marschall, H.R., Altherr, R., Gméling, K., Kasztovszky, Z., 2009. Lithium, boron and chlorine as tracers for metasomatism in high-pressure metamorphic rocks: a case study from Syros (Greece). Mineral. Petrol., 95, 291-302.

McCulloch, M.T., Gregory, R.T., Wasserburg, G.J. and Taylor, H.P., 1980. A neodymium, strontium, and oxygen isotopic study of the Cretaceous Samail ophiolite and implications for the petrogenesis and seawater-hydrothermal alteration of oceanic crust. Earth Planet. Sci. Lett., 46, 201-211.

Miller, C., Stosch, H.-G. and Hoernes, S., 1988. Geochemistry and origin of eclogites from the type locality Koralpe and Saualpe, Eastern Alps, Austria. Chem. Geol., 67, 103-118.

Miller, D.P., Marschall, H.R. and Schumacher, J.C., 2009. Metasomatic formation and petrology of blueschist-facies hybrid rocks from Syros (Greece): Implications for reactions at the slab-mantle interface. Lithos, 107, 53-67.

Miller, J.A., Cartwright, I., Buick, I.S. and Barnicoat, A.C., 2001. An O-isotope profile through the HP-LT Corsican ophiolite, France and its implications for fluid flow during subduction. Chem. Geol., 178, 43-69.

Molina, J.F. and Poli, S. Carbonate stability and fluid composition in subducted oceanic crust: an experimental study on H_2O-CO_2-bearing basalts. Earth Planet. Sci. Lett., 176, 295-310.

Mühlenbachs, K. and Clayton, R.N., 1976. Oxygen isotope composition of oceanic crust and its bearing on seawater. J. Geophys. Res., 81 (23), 4356-4369.

Nabelek, P.I., Labotka, T.C., O'Neil, J.R. and Papike, J.J., 1984. Contrasting fluid/rock interaction between Notch Peak granitic intrusion and argilites and limestones in western Utah: evidence from stable isotopes and phase assemblages. Contrib. Mineral. Petrol., 86, 25-34.

Pack, A., Toulouse, C. and Przybilla, R., 2007. Determination of oxygen triple isotope ratios without cryogenic separation of NF3 - technique with application to analyses of technical O2 gas and meteorite classification. Rapid Commun. Mass Spectrom., 21, 3721-3728.

Peacock, S.M., 1993. Large-scale hydration of the lithosphere above subducting slabs. Chem. Geol., 108, 49-59.

Pearce, J.A., 2008. Geochemical fingerprinting of oceanic basalts with applications to ophiolite classification and the search for Archean oceanic crust. Lithos, 100, 14-48.

Peate, D.W. et al., 1997. Geochemical variations in Vanuatu arc lavas: the role of subducted material and a variable mantle wedge composition. J. Petrol., 38, 1331-1358.

Penniston-Dorland, S.C., Sorensen, S.S., Ash, R.D. and Khadke, S.V., 2010. Lithium isotopes as a tracer of fluids in a subduction zone mélange: Franciscan Complex, CA. Earth Planet. Sci. Lett., 292, 181-190.

Plank, T. and Langmuir, C.H., 1993. Tracing trace elements from sediment input to volcanic output at subduction zones. Nature, 362, 739-743.

Plank, T. and Langmuir, C.H., 1998. The chemical composition of subducting sediment and its consequences for the crust and mantle. Chem. Geol., 145, 325-394.

Putlitz, B., Matthews, A. and Valley, J.W., 2000. Oxygen and hydrogen isotope study of high-pressure metagabbros and metabasalts (Cyclades, Greece): implications for the subduction of oceanic crust. Contrib. Mineral. Petrol., 138, 114-126.

Putnis, A. and John, T., 2010. Replacement processes in the Earth's Crust. Elements, 6, 159-164.

Ranero, C.R., Phipps Morgan, J., McIntosh, K. and Reichert, C., 2003. Bending-related faulting and mantle serpentinization at the Middle American trench. Nature, 425, 367-373.

Rüpke, L., Phipps Morgan, J., Hort, M. and Connolly, J.A.D., 2002. Are the regional variations in Central American arc lavas due to differing basaltic versus peridotitic slab sources of fluids? Geology, 30, 1035-1038.

Sadofsky, S.J. and Bebout, G.E., 2004. Field and isotopic evidence for fluid mobility in the Franciscan Complex: Forearc paleohydrogeology to depths of 30 kilometers. Int. Geol. Rev., 46, 1053-1088.

Salters, V.J.M. and Stracke, A., 2004. Composition of the depleted mantle. Geochem. Geophys. Geosyst., 5, Q05004, doi:10.1029/2003GC000597.

Savin, S.M. and Epstein, S., 1970. The oxygen and hydrogen isotope geochemistry of ocean sediments and shales. Geochim. Cosmochim. Acta, 34, 43-63.

Scambelluri, M. and Philippot, P., 2001. Deep fluids in subduction zones. Lithos, 55, 213-227.

Scambelluri, M., Hermann, J., Morten, L. and Rampone, E., 2006. Melt- versus fluid-induced metasomatism in spinel to garnet wedge peridotites (Ulten Zone, Eastern Italian Alps): clues from trace element and Li abundances. Contrib. Mineral. Petrol., 151, 372-394.

Scheele, N. and Hoefs, J., 1992. Carbon isotope fractionation between calcite, graphite and CO2: an experimental study. Contrib. Mineral. Petrol., 112, 35-45.

Schroeder, T., John, B. and Frost, B.R., 2002. Geologic implications of seawater circulation through peridotite exposed at slow-spreading mid-ocean ridges. Geology, 30, 367-370.

Sengör, A.C. and Natal'in, B.A., 1996. Paleotectonics of Asia: fragments of a synthesis. In: A. Yin and M. Harrison (Editors), The tectonic evolution of Asia. Cambridge University Press, Cambridge, pp. 486-640.

Sengör, A.M.C., Natal'in, B.A., Burtman, V.S., 1993. Evolution of the Altaid tectonic collage and Palaeozoic crustal growth in Eurasia. Nature, 364, 299-307.

Sharp, Z.D., 1990. A laser-based microanalytical method for the in situ determination of oxygen isotope ratios of silicates and oxides. Geochim. Cosmochim. Acta, 54, 1353-1357.

Sharp, Z., 2007. Principles of Stable Isotope Geochemistry. Pearson Prentice Hall, Upper Saddle River, New Jersey, 344 pp.

Shaw, H.F. and Wasserburg, G.J., 1985. Sm-Nd in marine carbonates and phosphates: Implications for Nd isotopes in seawater and crustal ages. Geochim. Cosmochim. Acta, 49, 503-518.

Singer, B.S. et al., 2007. Along-strike trace element and isotopic variation in Aleutian Island arc basalt: Subduction melts sediments and dehydrates serpentine. J. Geophys. Res., 112, B06206, doi:10.1029/2006JB004897.

Snow, J.E. and Reisberg, L., 1995. Os isotopic systematics of the MORB mantle: results from altered abyssal peridotites. Earth Planet. Sci. Lett., 133, 411-421.

Snow, J.E., Hart, S.R. and Dick, H.J.B., 1994. Nd and Sr isotope evidence linking mid-ocean-ridge basalts and abyssal peridotites. Nature, 371, 57-60.

Sorensen, S.S. and Grossman, J.N., 1989. Enrichment of trace elements in garnet amphibolites from a paleo-subduction zone: Catalina Schist, southern California. Geochim. Cosmochim. Acta, 53, 3155-3177.

Sorensen, S.S., Grossman, J.N. and Perfit, M.R., 1997. Phengite-hosted LILE enrichment in eclogite and related rocks: implications for fluid-mediated mass transfer in subduction zones and arc magma genesis. J. Petrol., 38, 3-34.

Spandler, C., Pettke, T. and Rubatto, D., 2011. Internal and external fluid sources for eclogite-facies veins in the Monviso meta-ophiolite, Western Alps: Implications for fluid flow in subduction zones. J. Petrol., 52, 1207-1236.

Spandler, C., Hermann, J., Arculus, R. and Mavrogenes, J., 2003. Redistribution of trace elements during prograde metamorphism from lawsonite blueschist to eclogite facies; implications for deep subduction-zone processes. Contrib. Mineral. Petrol., 146, 205-222.

Spandler, C., Hermann, J., Arculus, R. and Mavrogenes, J., 2004. Geochemical heterogeneity and element mobility in deeply subducted oceanic crust; insights from high-pressure mafic rocks from New Caledonia. Chem. Geol., 206, 21-42.

Spandler, C., Hermann, J., Faure, K., Mavorgenes, J.A. and Arculus, R.J., 2008. The importance of talc and chlorite "hybrid" rocks for volatile recycling through subduction zones; evidence from the high-pressure subduction mélange of New Caledonia. Contrib. Mineral. Petrol., 155, 181-198.

Staudigel, H., 2003. Hydrothermal alteration processes in the oceanic crust. In: R.L. Rudnick (Editor), The Crust. Treatise on Geochemistry. Elsevier-Pergamon, Oxford, pp. 511-536.

Staudigel, H., Davies, G.R., Hart, S.R., Marchant, K.M. and Smith, B.M., 1995. Large-scale isotopic Sr, Nd, and O isotopic composition of altered oceanic crust at DSDP/ODP Sites 417/418. Earth Planet. Sci. Lett., 130, 169-185.

Staudigel, H., Plank, T., White, W.M. and Schmincke, H.-U., 1996. Geochemical fluxes during seafloor alteration of the upper oceanic crust: DSDP sites 417 and 418. In: G.E. Bebout and S.H. Kirby (Editors), Subduction: Top to Bottom. American Geophysical Union, Washington, DC, pp. 19-38.

Stolper, E. and Newman, S., 1994. The role of water in the petrogenesis of Mariana trough magmas. Earth Planet. Sci. Lett., 121, 293-325.

Sun, S.-S. and McDonough, W.F., 1989. Chemical and isotopic systematics of oceanic basalts: implications for mantle composition and processes. In: A.D. Saunders and M.J. Norry (Editors), Magmatism in the Ocean Basins. Geological Society, London, Special Publication, pp. 313-345.

Tatsumi, Y., 1989. Migration of fluid phases and genesis of basalt magmas in subduction zones. J. Geophys. Res., 94(B4), 4697-4707.

Taylor, S.R. and McLennan, S.M., 1985. The continental crust: its composition and evolution. Blackwell, Oxford.

Valley, J.W., Kitchen, N., Kohn, M.J., Niendorf, C.R. and Spicuzza, M.J., 1995. UWG-2, a garnet standard for oxygen isotope ratios: Strategies for high precision and accuracy with laser heating. Geochim. Cosmochim. Acta, 59, 5223-5231.

van der Straaten, F., 2008. Retrogression of eclogites to blueschists: a record of fluid infiltration during uplift in subduction zones, Christian-Albrechts-Universität, Kiel, 142 pp.

van der Straaten, F., Schenk, V., John, T. and Gao, J., 2008. Blueschist-facies rehydration of eclogites (Tian Shan, NW-China): implications for fluid-rock interaction in the subduction channel. Chem. Geol., 225, 195-219.

Veizer, J., 1989. Strontium isotopes in seawater through time. Annual Review of Earth and Planetary Sciences, 17, 141-167.

Volkova, N.I. and Budanov, V.I., 1999. Geochemical discrimination of metabasalt rocks of the Fan-Karategin transitional blueschist/greenschist belt, South Tianshan, Tajikistan; seamount volcanism and accretionary tectonics. Lithos, 47, 201-216.

Vroon, P.Z., van Bergen, M.J., Klaver, G.J. and White, W.M., 1995. Strontium, neodymium, and lead isotopic and trace-element signatures of the East Indonesian sediments: Provenance and implications for Banda Arc magma genesis. Geochim. Cosmochim. Acta, 59, 2573-2598.

Windley, B.F., Allen, M.B., Zhang, C., Zhao, Z.-Y. and Wang, G.-R., 1990. Paleozoic accretion and Cenozoic redeformation of the Chinese Tien Shan Range, central Asia. Geology, 18, 128-131.

Xu, G., Frey, F.A., Weis, D., Scoates, J.S. and Giret, A., 2007. Flood basalts from Mt. Capitole in the central Kerguelen Archipelago: Insights into the growth of the archipelago and source components contributing to plume-related volcanism. Geochem. Geophys. Geosyst., 8, Q06007, doi:10.1029/2007GC001608.

Yang, H.-J. et al., 1998. Petrogenesis of the flood basalts forming the Northern Kerguelen Archipelago: implications for the Kerguelen plume. J. Petrol., 39, 711-748.

Yui, T.-F., Rumble, D., Chen, C.-H. and Lo, C.-H., 1997. Stable isotope characteristics of eclogites from the ultra-high-pressure metamorphic terrain, east-central China. Chem. Geol., 137, 135-147.

Zack, T. and John, T., 2007. An evaluation of reactive fluid flow an trace element mobility in subducting slabs. Chem. Geol., 239, 199-216.

Zack, T., Rivers, T, Foley, S. (2001). Cs-Rb-Ba systematics in phengite and amphibole: an assessment of fluid mobility at 2.0 GPa in eclogites from Trescolmen, Central Alps. Contributions to Mineralogy and Petrology, 140, 651-669.

Zheng, Y.-F., 1993a. Calculation of oxygen isotope fractionation in anhydrous silicate minerals. Geochim. Cosmochim. Acta, 57, 1079-1091.

Zheng, Y.-F., 1993b. Calculation of oxygen isotope fractionation in hydroxyl-bearing silicates. Earth Planet. Sci. Lett., 120, 247-263.

Zheng, Y.-F., Fu, B., Gong, B. and Li, L., 2003. Stable isotope geochemistry of ultrahigh pressure metamorphic rocks from the Dabie-Sulu orogen in China, implications for geodynamics and fluid regime. Earth Sci. Rev., 62, 105-161.

Zheng, Y.-F., Fu, B., Xiao, Y., Li, Y. and Gong, B., 1999. Hydrogen and oxygen isotope evidence for fluid-rock interactions in the stages of pre- and post-UHP metamorphism in the Dabie Mountains. Lithos, 46, 677-693.

Zheng, Y.-F., Gong, B., Li, Y. and Fu, B., 2000. Carbon concentrations and isotopic ratios of eclogites from the Dabie and Sulu terranes in China. Chem. Geol., 168, 291-305.

Figure captions

Fig. 1: Simplified geological and metamorphic map of the Chinese South Tian Shan modified after Gao et al. (1999). Stars indicate sample areas.

Fig. 2: Field photographs and sketches of blueschist-facies overprinted eclogites from the Chinese South Tian Shan. A) Eclogite and blueschist sample sequence FTS 9-1 in the Akanzayi River valley (left) and schematic illustration of drill holes (right). Note the whitish quartz vein at the contact of eclogite to meta-acidite. B) Pillow metabasalts in the Atantayi River valley (left) and schematic drawing of the eclogite and two distinct blueschist shells (right). Used samples are not displayed in Figure.

Fig. 3: Photomicrographs of eclogite and blueschist overprint of the FTS 9-1 sample sequence. A) Eclogite-facies assemblage of garnet (Grt), omphacite (Omp), rutile (Rt) and Cr-rich phengite (Phe). Beginning blueschist-facies overprint assemblage consists of amphibole (Amph), paragonite (Pg) and titanite (Ttn). B) Advanced blueschist-facies overprint with formation of paragonite, glaucophane (Gln), calcite (Cal) and titanite at the expense of garnet, omphacite and rutile.

Fig. 4: A) Chondrite-normalized (chondritic values from Boynton, 1984) REE diagram and B) N-MORB-normalized (values from Sun & McDonough, 1989) trace element diagram representative HP metamorphic rocks from the Tian Shan. Tholeiitic OIB (BHVO-1; preferred values from the GeoReM website) and back-arc basalt (BAB; sample MLM-7 from Vanuatu; Peate et al., 1997) are shown for comparison. Note the similarities of samples FTS 9-1.5A, FTS 1-26 and FTS 5-6 with BBB, N-MORB and tholeiitic OIB, respectively. C) Th/Yb vs. Nb/Yb diagram to identify the tectonic setting of metabasalts after Pearce (2008). N-MORB, E-MORB and alkalic OIB are from Sun & McDonough (1989), oceanic island arc basalt (IAB) is from Kelemen et al. (2003) and other comparative compositions as above. Note that the pillow metabasalts (data from van der Straaten et al., 2008) plot near the composition of tholeiitic OIB.

Fig. 5: A) C-O isotope diagram for carbonates from Tian Shan (TS) HP metabasalts and other subduction-related metamorphic rocks. The field for mantle carbon is from Des Marais and Moore (1984) and Kyser et al. (1982). The average $\delta^{13}C$ of sedimentary inorganic carbon is

from Sharp (2007). Note that organic carbon typically has $\delta^{13}C$ values from -40 to -20‰ (Sharp, 2007). Cc = calcite. Data sources: Norwegian (NOR) eclogites: Agrinier et al. (1985); Catalina Schist (CS): Bebout (1995); Calcite veins, Franciscan: Sadofsky and Bebout (2004); Alpine ophiolites: Cartwright and Barnicoat (1999); Corsican ophiolite: Miller et al. (2001); Calcite from AOC: Alt et al. (1985). B) $\delta^{18}O$ values of mineral separates from the Tian Shan rocks (filled black circles) compared to separated minerals from HP metabasalts from the Cyclades (grey circles; Putlitz et al., 2000) and Ecuador (open circles; Halama et al., 2011). Data for low-temperature AOC are from Gregory and Taylor (1981) and Cocker et al. (1982). The composition of fresh MORB glass is from Eiler et al. (2000).

Fig. 6: Oxygen isotope thermometry for blueschist-facies (A, C) and mixed eclogite-blueschist-facies (B, D) mineral assemblages of the Tianshan samples. Blueschist-facies assemblages of samples FTS 9-1 (A) and FTS 4-1.1 (pillow metabasalt, C) yield average temperatures of ~600 °C. No reasonable temperatures can be obtained for the mixed assemblages of FTS 9-1 (B, including eclogite-facies phengite and omphacite) and FTS 4-2.4 and FTS 4-3.5 (D). Fractionation curves between mineral pairs were calculated based on the mineral-water fractionation factors from Zheng (1993 a, b). In A and C, thick black lines represent the average temperature of the three carbonate-silicate equilibria and the white mica-garnet and glaucophane-garnet equilibria. The temperature of the white mica – glaucophane pairs was not considered in the calculation of the average because of the very small equilibrium fractionation at these temperatures, which translates into a significant error (>100 °C) of the calculated temperature due to the analytical uncertainty (± 0.2‰). The width of the rectangles in A and C reflects the uncertainty in the fractionation. Thin grey lines show ± 1 standard deviation of the average temperature. For B and D, the labels in italics denote the mineral pairs analyzed. Grey symbols indicate mineral pairs that are too far from equilibrium to yield a meaningful temperature estimate. Note the different temperature scales in B and D compared to A and C.

Fig. 7: Isochron diagrams of FTS samples. A) Rb-Sr-isochron diagram of blueschists from the pillow metabasalts, yielding a well-defined isochron age of 320±11 Ma. B) Rb-Sr-isochron of eclogites from the pillow metabasalts, yielding an errorchron with a slope corresponding to an age of 308±50 Ma. Both Rb-Sr-isochrons were calculated using errors of 5% for $^{87}Rb/^{86}Sr$ and 0.0025% on $^{87}Sr/^{86}Sr$. C) Sm-Nd isochron diagram of eclogites and blueschists from the FTS 4 pillow metabasalts. The errorchron age of 330±120 Ma is consistent with the Rb-Sr

ages, indicating equilibration of the Sm-Nd system at the time of metamorphism. D) Sm-Nd isochron diagram of blueschists and eclogites from the FTS 9-1 sequence. The data yield an errorchron age of 600±140 Ma. For both Sm-Nd-isochrons, assumed errors are 1% on $^{147}Sm/^{144}Nd$ and 0.001% on $^{143}Nd/^{144}Nd$.

Fig. 8: Sr-Nd isotope diagram for Tian Shan samples. Initial isotopic ratios for all mélange rocks and the FTS 4 samples (pillow metabasalts) were back calculated to 320 Ma. Note that initial isotopic ratios for the FTS 9-1 blueschist-eclogite transition are shown for 320 and 600 Ma. Isotopic ratios of recent oceanic basalts were not back calculated, but doing so would move the fields to the left and hence increase the isotopic differences to the Tianshan rocks. The composition of the depleted mantle (DM) at 320 and 600 Ma was calculated assuming a linear evolution for εNd (Goldstein et al., 1984) and using a present-day composition of $^{87}Rb/^{86}Sr = 0.046$ and $^{87}Sr/^{86}Sr = 0.7026$ (Taylor and McLennan, 1985). The composition of the Chondritic Uniform Reservoir (CHUR) was recalculated using $(^{87}Sr/^{86}Sr)_{BSE\_today}=0.7045$ and $(^{87}Rb/^{86}Sr)_{BSE\_today}=0.0827$ (DePaolo, 1988). Sources of comparative data: Oceanic island basalts (OIB), Kerguelen – Yang et al., 1998 and Xu et al., 2007; OIB, Samoa – Jackson et al., 2007; AOC, Canary Islands – Hoernle, 1998; Clinopyroxene and whole rocks data from oceanic peridotites – Snow et al., 1994 and Snow and Reisberg, 1995. Uncertainties in the isotopic values are smaller than the symbol size.

Fig. 9: A) and B) Trace element diagrams of Tian Shan HP rocks commonly used to distinguish between HP/UHP metasomatic effects and seafloor alteration (after Bebout 2007). C) Ba vs. K_2O diagram illustrating the geochemical similarity of the blueschist-facies overprint in the FTS 9-1 sequence to the enrichment of these elements in island arc rocks compared to N-MORB. D) Enrichment of Ni and Co in overprinted FTS 9-1 rocks compared to eclogitic precursors and typical orogenic serpentinites. Data for the FTS 4 samples are from van der Straaten et al. (2008). N-MORB and OIB compositions are from Sun & McDonough (1989). AOC 417/418 and AOC 801 are the super composites from Staudigel et al. (1996) and Kelley et al. (2003), respectively. The composition of the Depleted MORB mantle (DMM) is from Salters and Stracke (2004), serpentinite data are from Hattori and Guillot (2003). EC = Eclogite, PAB = Phengite-ankerite blueschist, GBs = Glaucophane-dominated blueschist.

Fig. 10: A) Systematic enrichment and depletion of certain trace elements with increasing blueschist-facies overprint in the FTS 9-1 sequence. B) Systematic increase of trace element

ratios used as slab fluid tracers with increasing metasomatic overprint in the FTS 9-1 sequence. C) Isocon diagram using eclogite FTS 9-1.5A as least overprinted precursor and blueschist FTS 9-1.1. as most intensely overprinted rock. The slope of the isocon is based on immobility of Ti, P, Zr, Hf, Nb and Ta. Elements are scaled following the approach of Grant (2005), with the major element oxides on the right side, except for K_2O, and generally decreasing abundances from right to left.

Fig. 11: Model calculations for mixing of hypothetical precursor basalt with sediment-derived fluid (SED; red lines), fluid derived from seawater-altered oceanic lithosphere (SAOL; dashed lines) and slab fluids. Slab fluids are assumed to consist of 80% SAOL fluid and 20% SED1/SED2 fluid. The precursor compositions of the basaltic ocean crust are based on compositions of the eclogitic parts for [Sr], [Nd] and εNd. Initial Sr isotope compositions of the precursor basalts were estimated by assigning values that plot on the mantle array at the given εNd values. The two sediment end-members chosen for modeling are clay and chert from the Kurile arc (SED1) and terrigenous sediments from the Southern Antilles trench (SED2). The composition of seawater-altered oceanic lithosphere is taken from the estimated composition of seawater (Veizer, 1989; Shaw and Wasserburg, 1985). See Table 4 for details about the model parameters used in the calculations. Tick marks denote 10% steps. Data sources: Global subducted sediment – Plank and Langmuir, 1998; East Indonesian sediment – Vroon et al., 1995; Altered oceanic crust from the Samail ophiolite – McCulloch et al., 1980.

Fig. 12: Sketch illustrating the complexity of chemical and isotopic variations in the various lithologies present in the subduction channel at the slab-wedge interface and summarizing the contributions to the fluid-induced metasomatic overprint in the FTS 9-1 sequence (based on Bebout, 2007; Bebout and Barton, 1989; Breeding et al., 2004).

Table 1: Major and trace element data of Tian Shan metamorphic rocks

Sample name	FTS 9-1.1	FTS 9-1.2	FTS 9-1.3B	FTS 9-1.3A	FTS 9-1.4	FTS 9-1.5B	FTS 9-1.5 A	FTS 9-1.6	FTS 9-1.8	FTS 9-1.9	FTS 9-1.11	FTS 9-1.12	FTS 1-26	FTS 2-15	FTS 5-6	FTS 6-5B
Rock type	Blueschist	Blueschist	EC/BS	EC/BS	EC/BS	EC/BS	Eclogite	Eclogite	Vein	Meta-Acidite	Meta-Acidite	Meta-Acidite	Eclogite	Grt-mica-schist	Blueschist	Fuchsite schist
Trace element analysis	CAU	CAU	CAU	CAU	CAU	CAU	CAU	CAU	ACME	ACME			ACME	ACME	ACME	ACME
Major elements (wt.%)																
SiO_2	47.23	39.43	36.43	42.03	41.17	43.65	49.75	55.14	87.97	67.29	64.02	68.70	49.56	67.97	46.58	51.26
TiO_2	0.65	0.75	0.44	0.58	0.68	0.59	0.64	0.23	0.13	0.52	0.50	0.42	1.35	0.59	2.02	0.75
Al_2O_3	13.26	12.77	9.48	12.15	12.60	11.93	12.52	10.66	5.38	13.03	15.01	12.94	12.33	13.32	13.45	19.33
Fe_2O_3	8.23	10.84	9.27	8.65	8.81	9.30	7.94	7.33	2.34	6.65	7.34	8.45	12.16	8.24	11.48	12.53
MnO	0.11	0.35	0.23	0.17	0.22	0.24	0.20	0.14	0.06	0.08	0.07	0.16	0.2	0.12	0.13	0.23
MgO	10.29	10.30	12.28	11.23	9.69	9.27	7.59	6.88	0.59	2.91	3.49	2.45	6.17	2.93	8.12	2.56
CaO	6.66	9.86	11.90	8.67	11.12	11.72	12.28	11.80	1.15	4.95	3.10	4.01	12.72	2.43	7.33	4.67
Na_2O	5.56	4.10	4.16	4.88	4.78	5.09	5.94	6.05	1.03	3.33	4.04	2.78	4.72	3.36	4.21	1.08
K_2O	0.28	0.31	0.16	0.24	0.15	0.10	0.08	0.02	0.07	0.14	1.06	0.15	0.05	0.31	0.26	3.68
P_2O_5	0.01	0.01	0.01	0.05	0.01	0.01	0.01	0.05	0.11	0.03	0.01	0.15	0.02	0.18	0.27	0.17
CO_2	7.34	11.76	n.a.	11.48	10.94	8.80	3.37	1.78	n.a.	n.a.	n.a.	n.a.	n.a.	n.a.	n.a.	n.a.
H_2O = LOI - CO_2	1.68	0.47	n.a.	1.34	0.50	0.34	0.10	0.06	n.a.	n.a.	n.a.	n.a.	n.a.	n.a.	n.a.	n.a.
LOI	9.02	12.23	17.61	12.82	11.44	9.14	3.47	1.84	0.87	1.39	1.07	0.49	-0.20	0.62	6.21	4.15
Total	**101.29**	**100.88**	**101.97**	**101.47**	**100.67**	**101.02**	**100.42**	**100.14**	**99.70**	**100.32**	**99.70**	**100.70**	**99.08**	**100.07**	**100.06**	**100.41**
Trace elements (ppm)																
Li	42.3	30.2	32.0	123.7	35.5	33.6	37.7	53.0	n.a.	n.a.	n.a.	n.a.	n.a.	n.a.	n.a.	n.a.
Sc	25.7	63.5	19.7	20.0	42.8	32.8	38.6	19.8	n.a.	n.a.	n.a.	n.a.	n.a.	n.a.	n.a.	n.a.
V	178	173	162	173	205	176	205	140	16	100	n.a.	n.a.	399	97	191	293
Cr*	1120	1206	763	1080	1147	993	1188	192	n.d.	6	n.d.	n.d.	130	n.d.	165	750
Co	49.2	50.9	55.6	56.6	48.4	47.1	32.4	31.1	2.9	9.1	n.a.	n.a.	30.6	12.9	40.3	36.2
Ni	369	396	361	420	404	349	231	194	4.9	1.7	n.a.	n.a.	28.5	2.5	37.3	151
Cu	19.5	66.6	84.4	67.4	63.1	63.9	44.9	60.2	4	6.4	n.a.	n.a.	49.9	9.7	25	43.8
Zn	100	75.1	78.8	85.3	62.1	64.0	51.6	52.2	4	6	n.a.	n.a.	13	23	29	50
Ga	15.1	12.3	10.1	13.0	13.3	13.3	15.9	15.0	4.3	12.7	n.a.	n.a.	16.5	13.8	18.6	18.0
Rb	5.70	6.25	3.09	4.81	2.31	1.67	1.65	0.64	0.4	0.9	n.a.	n.a.	1.3	3.6	5.2	74.5
Sr	301	412	496	448	412	316	159	84.5	129	276	n.a.	n.a.	33.4	197.5	233	135
Y	13.2	38.6	15.4	13.8	22.2	16.0	18.4	2.22	7.5	21.5	n.a.	n.a.	36.2	18.1	23.2	22.4
Zr	26.7	28.6	16.2	22.7	26.7	23.5	26.2	14.1	23.9	89.4	n.a.	n.a.	81.3	85.9	169	27.3
Nb	0.80	0.62	0.30	0.45	0.48	0.59	0.75	0.61	0.6	2.7	n.a.	n.a.	2.1	2.7	20.9	1.5
Mo	0.14	0.13	0.12	0.12	0.13	0.14	0.15	0.37	n.d.	n.d.	n.a.	n.a.	0.2	n.d.	0.8	n.d.
Sn	0.40	0.39	0.28	0.32	0.47	0.55	0.81	0.78	n.d.	2	n.a.	n.a.	n.d.	n.d.	2	1
Sb	0.06	0.04	0.04	0.06	0.04	0.04	0.05	0.06	n.d.	n.d.	n.a.	n.a.	0.1	n.d.	n.d.	n.d.
Cs	0.25	0.30	0.29	0.38	0.16	0.17	0.14	0.19	n.d.	n.d.	n.a.	n.a.	n.d.	0.1	0.6	2.7
Ba	102	120	65.7	92.8	49.7	34.1	30.5	7.39	18	34	n.a.	n.a.	18	131	56	854
La	0.20	0.58	0.28	0.41	1.72	2.86	2.14	1.06	3.0	4.7	n.a.	n.a.	2.3	6.0	19	2.2
Ce	0.64	1.86	0.83	1.28	4.47	7.28	5.64	2.75	7.4	12.2	n.a.	n.a.	7.1	15.6	44.2	3.8
Pr	0.12	0.36	0.16	0.24	0.78	1.19	0.92	0.44	1.12	1.8	n.a.	n.a.	1.25	2.13	5.45	0.62
Nd	0.71	2.14	0.92	1.45	4.37	6.15	4.73	2.23	5.3	8.7	n.a.	n.a.	7.0	9.6	24	3.1
Sm	0.32	0.93	0.50	0.64	1.73	2.07	1.57	0.67	1.45	2.35	n.a.	n.a.	2.74	2.38	5.25	1.12
Eu	0.17	0.43	0.33	0.31	0.77	0.95	0.72	0.28	0.6	0.82	n.a.	n.a.	1.01	0.59	1.63	0.48
Gd	0.78	1.97	1.52	1.31	2.64	2.74	2.33	0.67	1.67	2.66	n.a.	n.a.	4.59	2.68	5.18	2.4
Tb	0.24	0.59	0.40	0.33	0.54	0.46	0.44	0.08	0.24	0.48	n.a.	n.a.	0.92	0.48	0.81	0.54
Dy	2.06	5.40	2.72	2.39	3.79	2.79	3.00	0.40	1.29	3.26	n.a.	n.a.	5.87	3.13	4.46	3.74
Ho	0.47	1.33	0.54	0.50	0.78	0.55	0.63	0.08	0.26	0.74	n.a.	n.a.	1.29	0.69	0.86	0.87
Er	1.30	3.97	1.38	1.32	2.00	1.44	1.68	0.23	0.77	2.35	n.a.	n.a.	3.82	2.13	2.31	2.59
Tm	0.19	0.63	0.19	0.19	0.27	0.20	0.24	0.03	0.11	0.36	n.a.	n.a.	0.59	0.34	0.31	0.4
Yb	1.18	4.26	1.19	1.20	1.60	1.23	1.46	0.25	0.74	2.48	n.a.	n.a.	3.88	2.27	1.98	2.54
Lu	0.17	0.64	0.18	0.18	0.22	0.17	0.20	0.04	0.11	0.41	n.a.	n.a.	0.57	0.36	0.28	0.39
Hf	0.86	0.95	0.54	0.75	0.87	0.77	0.87	0.47	0.7	2.4	n.a.	n.a.	2.7	2.7	4.2	0.8
Ta	0.03	0.03	0.01	0.02	0.02	0.02	0.03	0.03	n.d.	0.2	n.a.	n.a.	0.1	0.2	1.3	n.d.
W	0.37	0.46	0.38	0.46	0.40	0.27	0.38	0.42	n.d.	0.6	n.a.	n.a.	n.d.	0.5	n.d.	1.1
Pb	3.16	3.85	4.39	4.43	3.68	2.64	1.52	0.91	0.7	1.1	n.a.	n.a.	0.7	1.3	2.3	5.9
Th	0.03	0.05	0.02	0.04	0.08	0.15	0.12	0.08	0.5	1.1	n.a.	n.a.	0.3	1.9	2.4	0.3
U	0.03	0.05	0.02	0.04	0.07	0.08	0.06	0.06	0.2	0.6	n.a.	n.a.	0.2	0.4	0.6	0.2

*analyzed by XRF
n.d. = not detected; n.a. = not analyzed
CAU = University of Kiel, Germany; ACME = ACME laboratories, Canada

Table 2: Oxygen and carbon isotope data of separated minerals from the Tian Shan metamorphic rocks

Sample	Rock type	Mineral	$\delta^{18}O_{V\text{-}SMOW}$ (‰)	$\delta^{13}C_{V\text{-}PDB}$ (‰)	Reaction time (min)
FTS 4-1.1	Blueschist	Grt	8.20		
		Gln	9.72		
		Phe	10.25		
		Ank	12.95	-1.56	18
FTS 4-2.4	EC/BS transition	Grt	8.66		
		Omp	9.63		
		Gln	9.08		
		Phe	11.55		
FTS 4.2-5A	AAV	Ank (powdered)	12.76	-2.17	18
FTS 4-2.5B	AAV	Ank (powdered)	12.82	-2.19	18
FTS 4-2.5C	AAV	Ank	13.29	-2.00	26
FTS 4-2.5D	AAV	Ank	13.22	-1.96	34
FTS 4-3.3	EC/BS transition	Omp	9.12		
		Gln	10.25		
FTS 4-3.5	EC/BS transition	Grt	8.71		
		Omp	9.68		
		Gln	9.61		
		Phe	10.54		
		Czo	9.13		
		Ank	13.13	-1.73	18
FTS 9-1.1	Blueschist	Cal	11.75	-9.40	4
FTS 9-1.2	Blueschist	Cal	11.44	-9.06	4
FTS 9-1.3	EC/BS transition	Cal	11.78	-9.13	4
FTS 9-1.4	EC/BS transition	Cal	11.82	-8.96	4
FTS 9-1.5	EC/BS transition	Grt	7.31		
		Omp	8.20		
		Gln	8.81		
		Phe	8.52		
		Pg	9.20		

EC/BS = Eclogite/blueschist; AAV = Ankerite-apatite vein;
Mineral abbreviations: Grt = garnet, Gln = glaucophane, Phe = phengite, Ank = ankerite, Omp = omphacite, Czo = clinozoisite, Cal = calcite, Pg = paragonite.

Table 3: Strontium and Nd isotope data of Tian Shan metamorphic rocks

Sample	Rock type	Preparation	Rb (ppm)	Sr (ppm)	$(^{87}Sr/^{86}Sr)_{m}$	2□	$^{87}Rb/^{86}Sr$	$(^{87}Sr/^{86}Sr)_{320\ Ma}$	$(^{87}Sr/^{86}Sr)_{600\ Ma}$	Sm (ppm)	Nd (ppm)	$(^{143}Nd/^{144}Nd)_{m}$	2□	$^{147}Sm/^{144}Nd$	$(^{143}Nd/^{144}Nd)_{320\ Ma}$	□$Nd_{320\ Ma}$	$(^{143}Nd/^{144}Nd)_{600\ Ma}$	□$Nd_{600\ Ma}$	□Nd_{0}
FTS 4 pilow metabasalts																			
FTS 4-1.1 Bs	PAB	solution	69.19	137.7	0.712869	0.000007	1.455	0.70624	0.70042	2.61	11.20	0.512654	0.000002	0.140	0.512361	2.6	0.512103	4.6	0.3
FTS 4-1.5 Ec	Eclogite	solution	29.82	356.2	0.707226	0.000006	0.242	0.70612	0.69084	6.88	28.40	0.512662	0.000003	0.146	0.512357	2.6	0.512091	4.4	0.5
FTS 4-1.5 Bs	GBs	solution	57.21	43.98	0.723093	0.000005	3.770	0.70592	0.70515	5.52	23.50	0.512647	0.000003	0.141	0.512351	2.4	0.512089	4.4	0.2
FTS 4-2.4 Ec	Eclogite	solution	46.42	251.0	0.708644	0.000005	0.535	0.70621	0.69881	6.55	27.30	0.512654	0.000003	0.144	0.512351	2.4	0.512106	4.7	0.3
FTS 4-2.4 Bs	PAB	solution	63.73	98.17	0.714895	0.000005	1.880	0.70633	0.70407	8.68	38.30	0.512642	0.000003	0.136	0.512356	2.5	0.512086	4.3	0.1
FTS 4-2.5 Karb	AAV	solution	0.056	706.9	0.706102	0.000006	0.0002	0.70610	0.70610	1.43	3.70	0.512823	0.000008	0.233	0.512336	2.1	0.511908	0.8	3.6
FTS 4-3.1 Ec	Eclogite	solution	24.77	183.5	0.708084	0.000006	0.391	0.70630	0.70138	4.45	18.68	0.512653	0.000002	0.143	0.512352	2.5	0.512099	4.6	0.3
FTS 4-3.1 Bs	PAB	solution	55.36	125.8	0.712275	0.000006	1.274	0.70647	0.70474	3.68	15.50	0.512661	0.000003	0.143	0.512361	2.6	0.512089	4.4	0.4
FTS 4-3.3 Ec	Eclogite	solution	7.23	402.4	0.706567	0.000005	0.052	0.70633	0.70282	5.24	21.60	0.512668	0.000002	0.146	0.512362	2.7	0.512081	4.2	0.6
FTS 4-3.3 Bs	PAB	solution	56.86	180.4	0.710629	0.000006	0.912	0.70647	0.70612	4.17	16.90	0.512665	0.000002	0.149	0.512353	2.5	0.512094	4.5	0.5
FTS 4-3.5 Ec	Eclogite	solution	4.97	245.9	0.706563	0.000005	0.058	0.70630	0.70606	4.58	18.70	0.512663	0.000002	0.147	0.512354	2.5	0.512083	4.3	0.5
FTS 4-3.5 Bs	GBs	solution	25.83	170.5	0.708318	0.000005	0.438	0.70632	0.70457	4.94	19.90	0.512672	0.000003	0.149	0.512359	2.6	0.512084	4.3	0.7
FTS 9-1 EC-BS transition																			
FTS 9-1.1	Blueschist	solution	5.70	300.7	0.707315	0.000006	0.055	0.70707	0.70685	0.32	0.71	0.513297	0.000003	0.272	0.512728	9.8	0.512229	7.1	12.8
FTS 9-1.2	Blueschist	powder	6.25	411.9	0.707307	0.000002	0.044	0.70711	0.70693	0.93	2.14	0.513331	0.000002	0.262	0.512782	10.9	0.512302	8.5	13.5
FTS 9-1.3A	EC/BS	powder	4.81	448.1	0.707237	0.000003	0.031	0.70710	0.70697	0.64	1.45	0.513317	0.000002	0.266	0.512759	10.4	0.512271	7.9	13.2
FTS 9-1.4	EC/BS	powder	2.31	412.2	0.707227	0.000003	0.016	0.70715	0.70709	1.73	4.37	0.513224	0.000002	0.238	0.512727	9.8	0.512290	8.3	11.4
FTS 9-1.5A-p	Eclogite	powder	1.65	158.7	0.707282	0.000003	0.030	0.70714	0.70702	1.57	4.73	0.513046	0.000003	0.200	0.512627	7.8	0.512259	7.7	8.0
FTS 9-1.5A-p_replicate	Eclogite	powder	1.65	158.7	0.707289	0.000002	0.030	0.70715	0.70703	1.57	4.73	0.513036	0.000003	0.200	0.512617	7.6	0.512249	7.5	7.8
FTS 9-1.5A-s	Eclogite	solution	1.65	158.7	0.707268	0.000006	0.030	0.70713	0.70701	1.57	4.73	0.513039	0.000003	0.200	0.512621	7.7	0.512254	7.6	7.8
FTS 9-1.5A (average)	Eclogite		1.65	158.7	0.707280		0.030	0.70714	0.70702	1.57	4.73	0.513040		0.200	0.512621	7.7	0.512254	7.6	7.8
FTS 9-1.6	Eclogite	solution	0.64	84.53	0.707266	0.000006	0.022	0.70717	0.70708	0.67	2.23	0.512980	0.000004	0.181	0.512601	7.3	0.512269	7.9	6.7
Other rocks																			
FTS 9-1.8	Vein	powder	0.4	129.1	0.707180	0.000003	0.009	0.70714	0.70710	1.45	5.3	0.512846	0.000002	0.165	0.512501	5.4	0.512198	6.5	4.1
FTS 9-1.9	Meta-acidite	powder	0.9	276.3	0.707230	0.000003	0.009	0.70719	0.70715	2.35	8.7	0.512838	0.000003	0.163	0.512498	5.3	0.512199	6.5	3.9
FTS 1-26	Eclogite	powder	1.3	33.40	0.708317	0.000003	0.113	0.70780	0.70735	2.74	7	0.513064	0.000003	0.236	0.512571	6.7	0.512138	5.3	8.3
FTS 5-6	Blueschist	powder	3.6	197.5	0.706639	0.000003	0.053	0.70640	0.70619	2.38	9.6	0.512518	0.000003	0.149	0.512206	-0.4	0.511932	1.3	-2.3
FTS 2-15	Grt-mica-schist	powder	5.2	232.5	0.706988	0.000002	0.065	0.70669	0.70643	5.25	24	0.512735	0.000003	0.132	0.512460	4.6	0.512218	6.9	1.9
FTS 6-5B	Fuchsite schist	powder	74.5	135.4	0.715755	0.000003	1.593	0.70850	0.70212	1.12	3.1	0.512945	0.000008	0.217	0.512489	5.1	0.512090	4.4	6.0

PAB = Phengite-ankerite blueschist; GBs = Glaucophane-dominated blueschist; AAV = Ankerite-apatite vein; EC/BS = Eclogite/Blueschist
Solution = sample solutions from ICP-MS trace element measurements; powder = newly dissolved whole-rock powders

Table 4: Model parameters used for mixing calculations

Component	Sr (ppm)	Nd (ppm)	$^{87}Sr/^{86}Sr$	□Nd
FTS 4 basalt	300	20	0.7040	2.5
FTS 9-1 basalt	160	5	0.7025	8
Sediment 1	22.0	16.6	0.71297	-5.8
Sediment 2	139	43.38	0.70986	-11.3
SAOL	120	6.5	0.7085	-6
$D_{SED-Fluid}$	0.53	3.3		
$D_{SAOL-Fluid}$	0.19	51		
SED fluid 1	39.8	5.22	0.71297	-5.8
SED fluid 2	251.1	13.6	0.70986	-11.3
SAOL fluid	520.6	0.13	0.7085	-6
Slab fluid 1	424.4	1.15	0.70858	-5.8
Slab fluid 2	466.7	2.83	0.70865	-11.1

SED 1 = Clay/chert from the Kurile arc (Plank and Langmuir, 1998)
SED 2 = Terrigenous sediment from the Southern Antilles arc (Plank and Langmuir, 1998)
SAOL = Seawater-altered oceanic lithosphere (values for AOC from Singer et al., 2007)
SED-fluid partition coefficients from Johnson and Plank (1999)
SAOL-fluid partition coefficients from Brenan et al. (1995)
Calculated composition of released fluid assumes 5% fluid in equilibrium with SED/SAOL
Composition of slab fluids assumes a 80:20 mixture of AOC fluid with SED1/SED2 fluid

Fig. 1

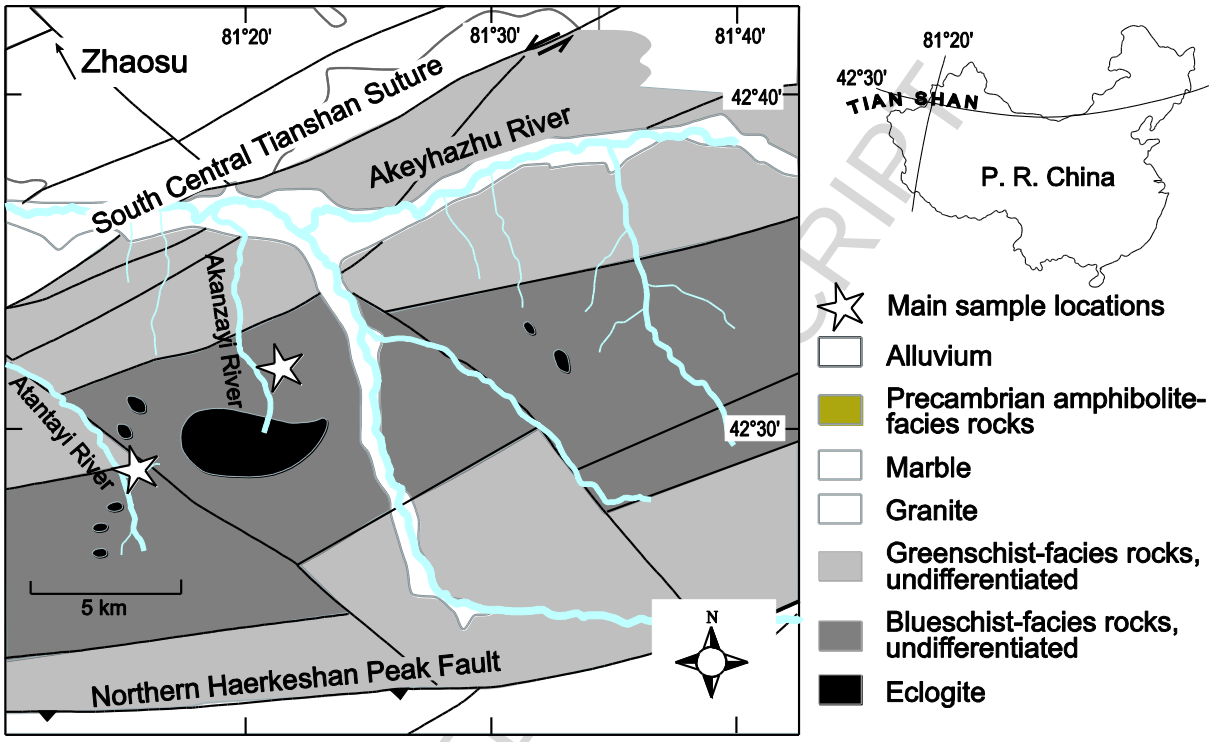

Fig. 2

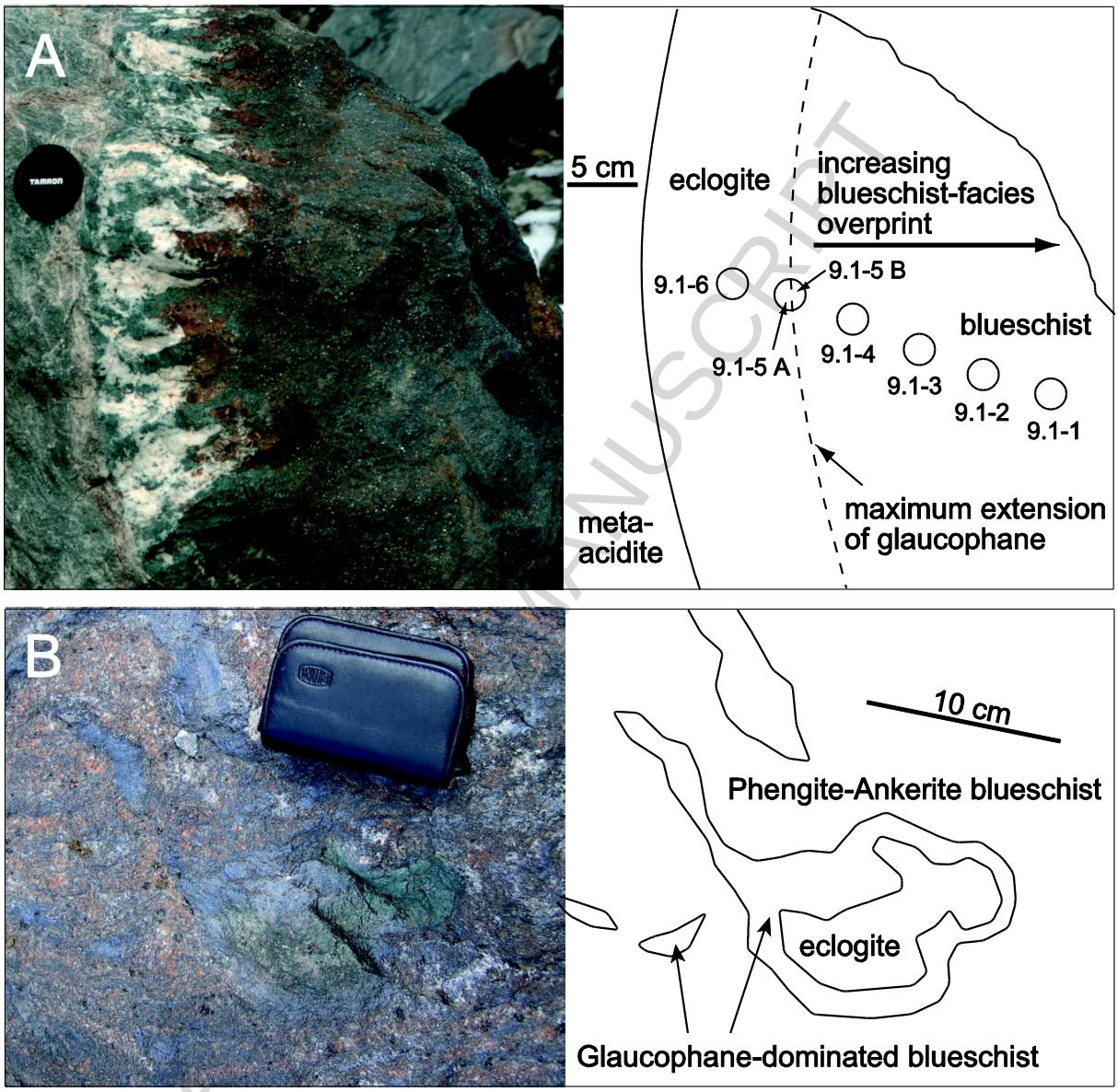

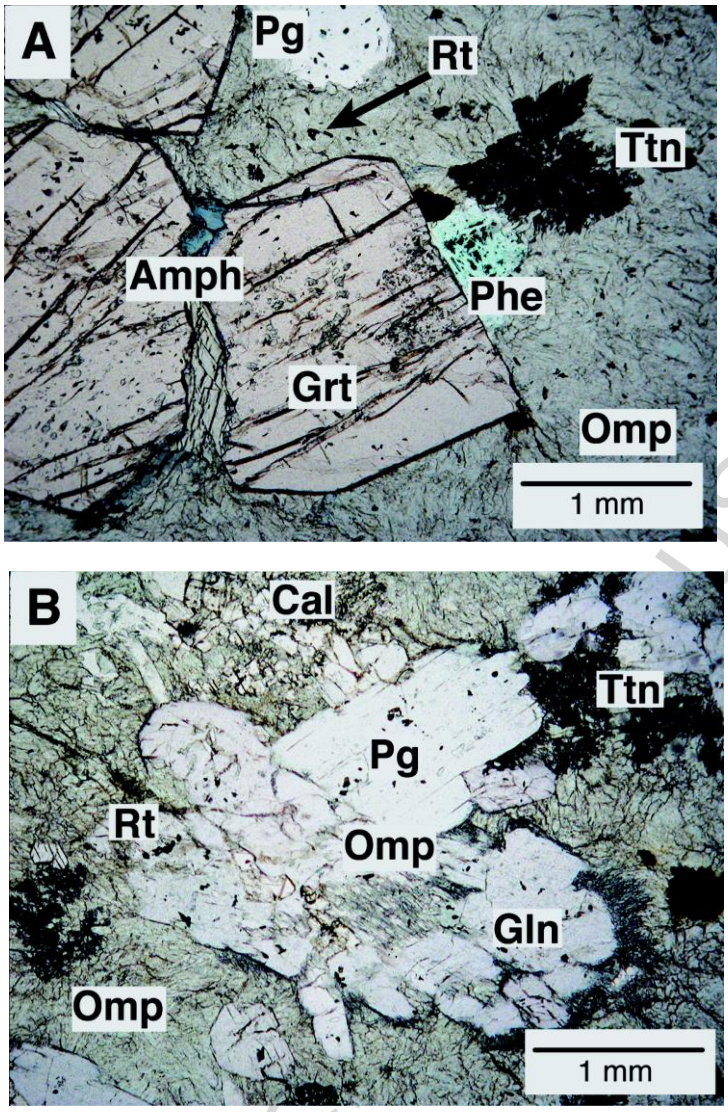

Fig. 3

Fig. 4

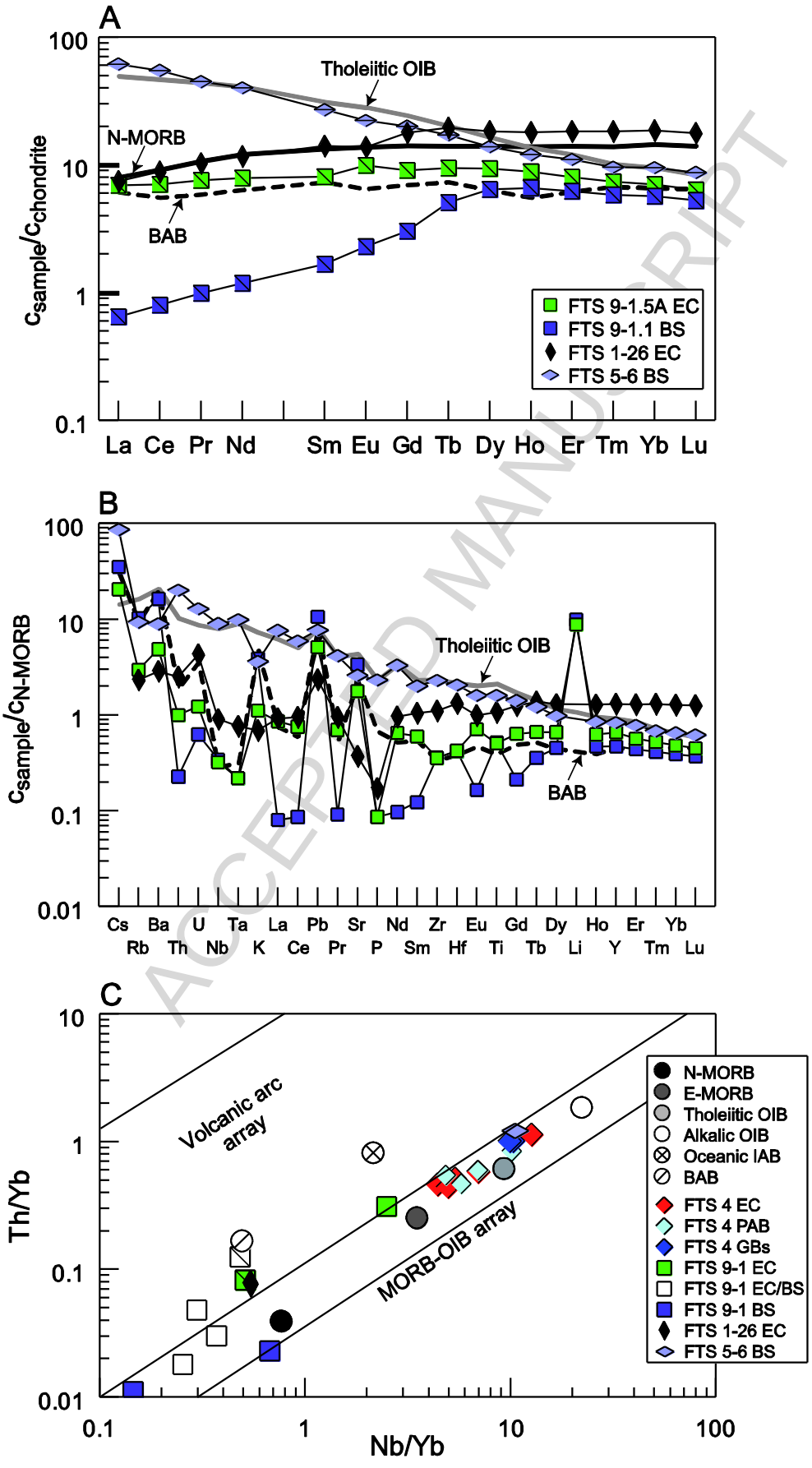

Fig. 5

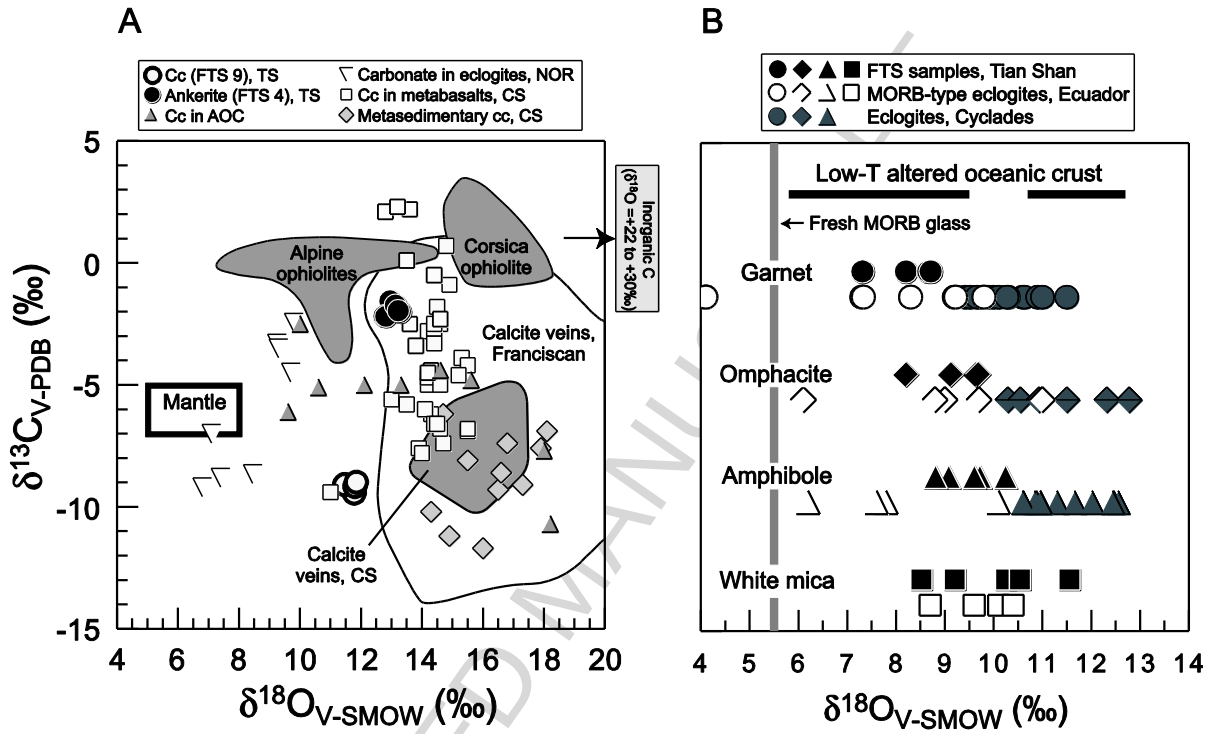

Fig. 6

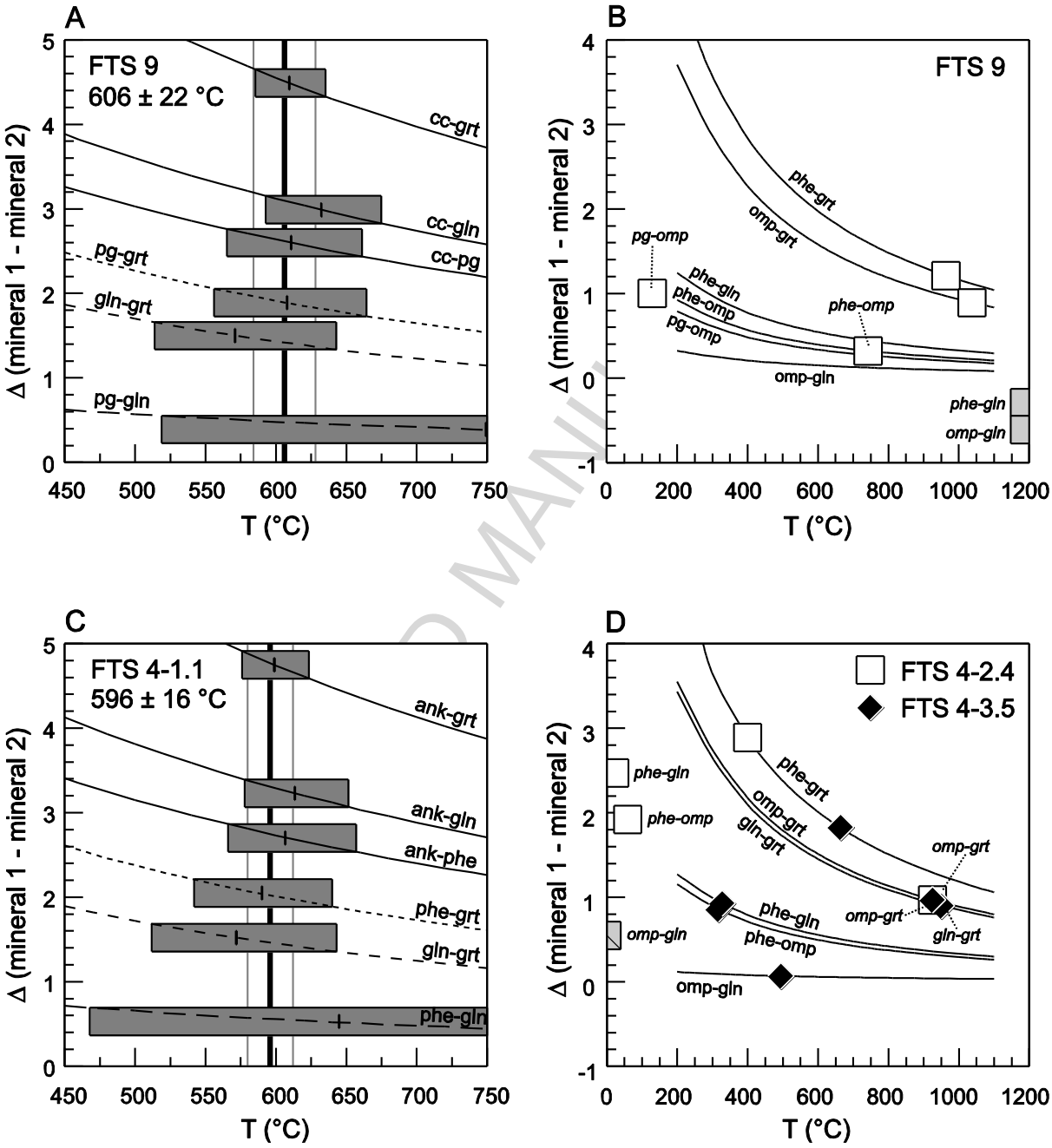

Fig. 7

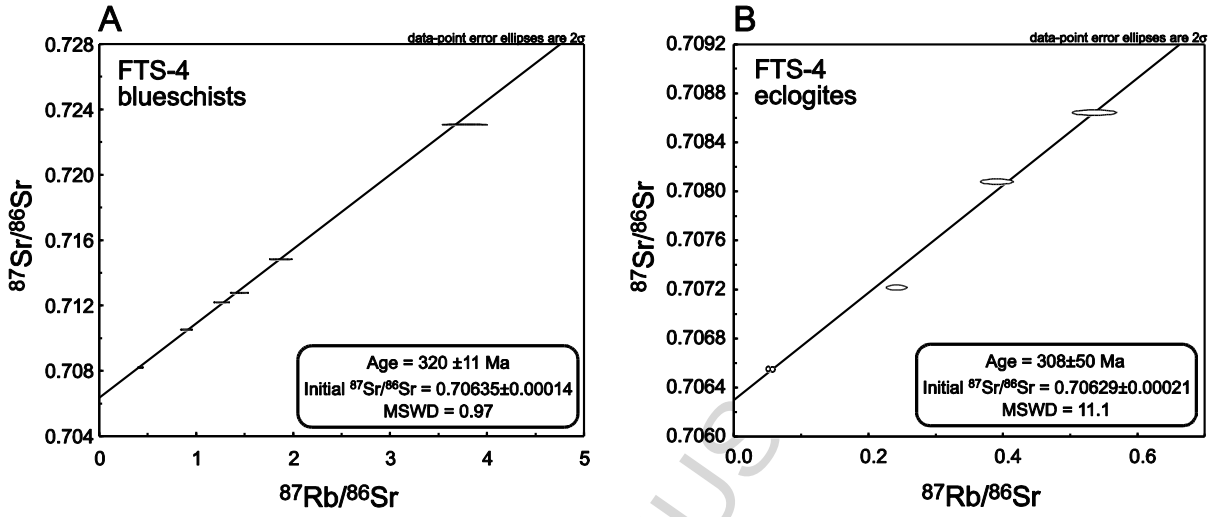

Fig. 8

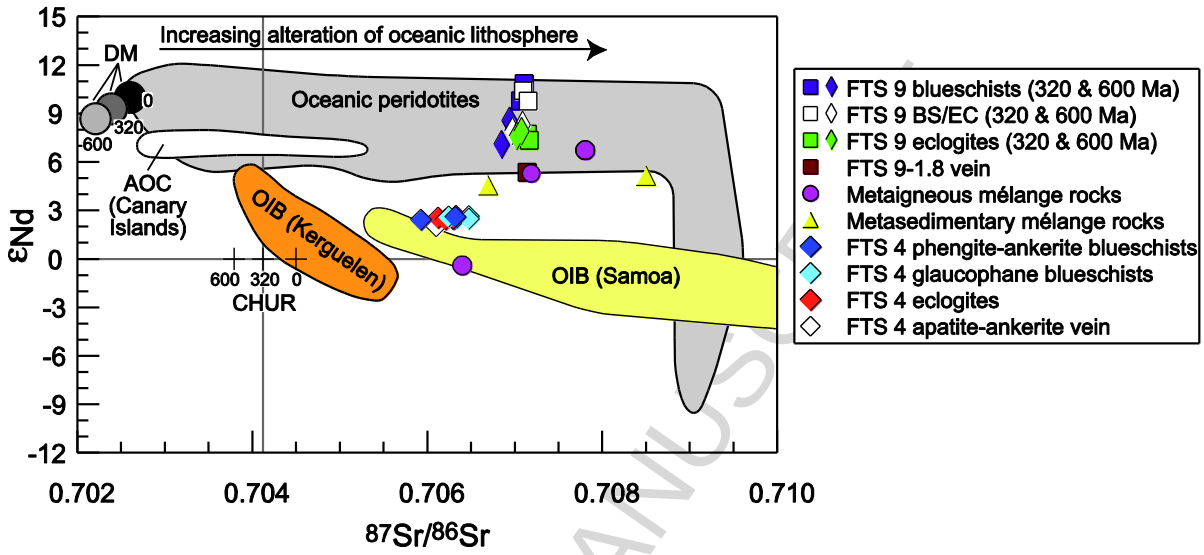

Fig. 9

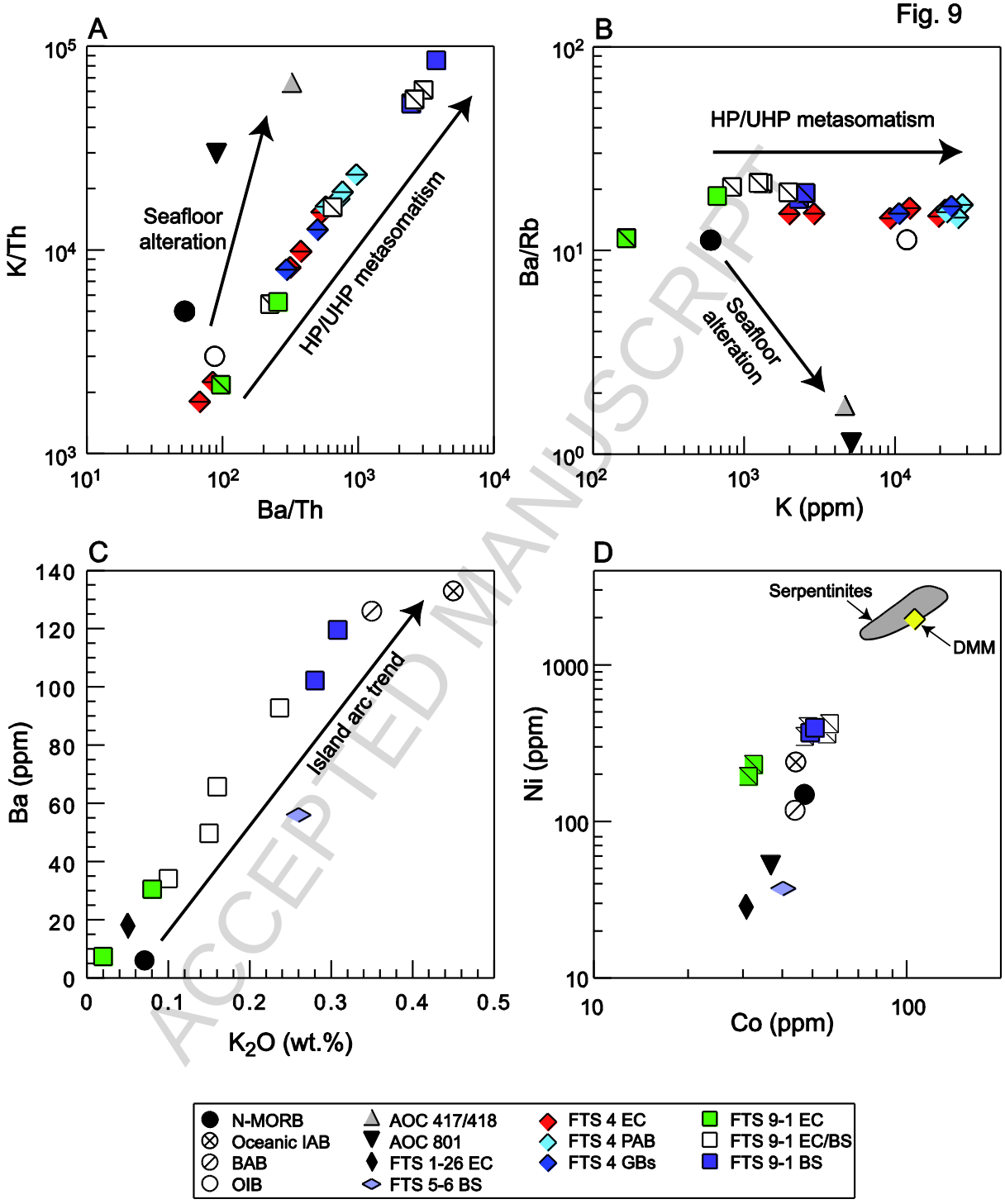

Fig. 10

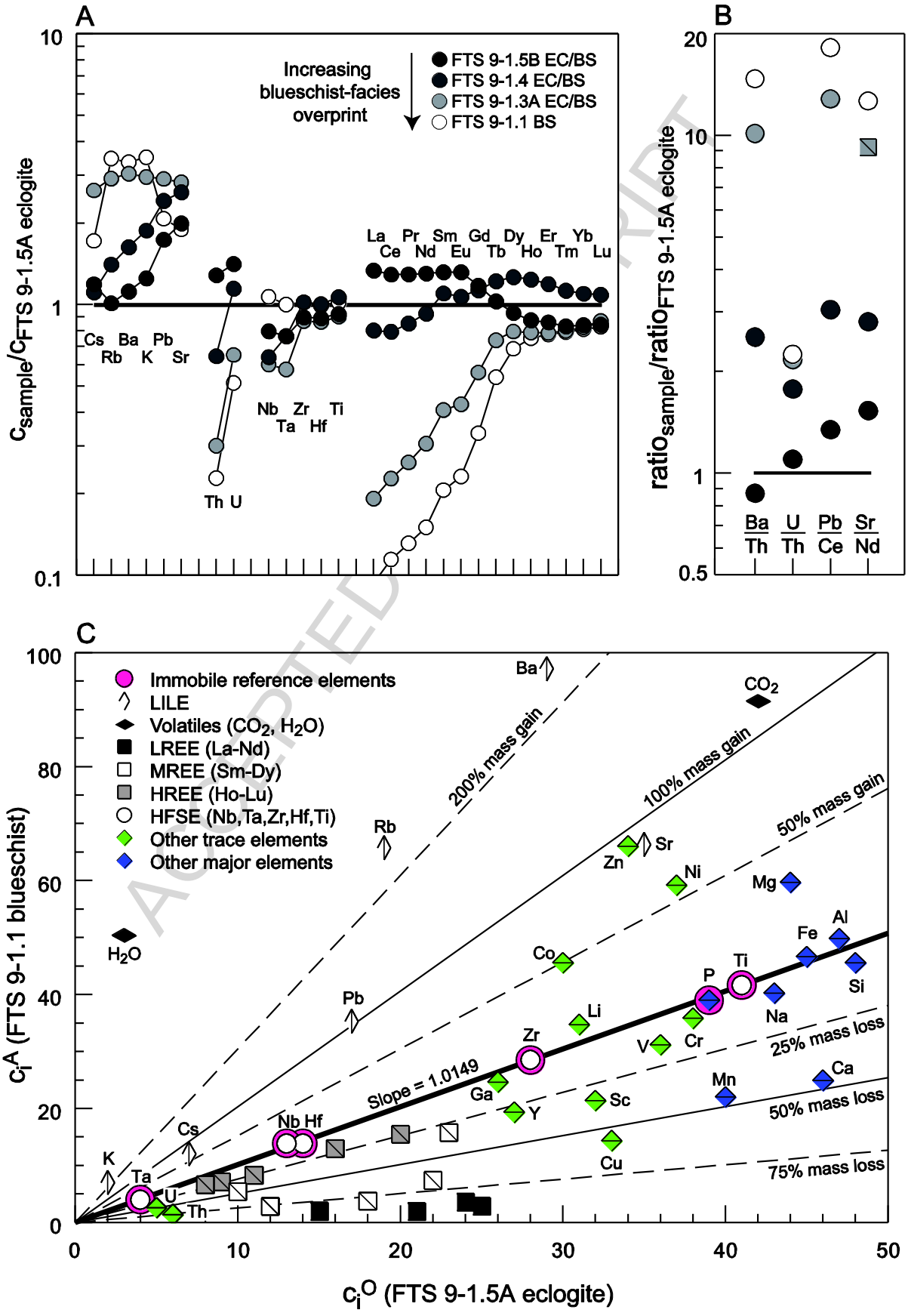

Fig. 11

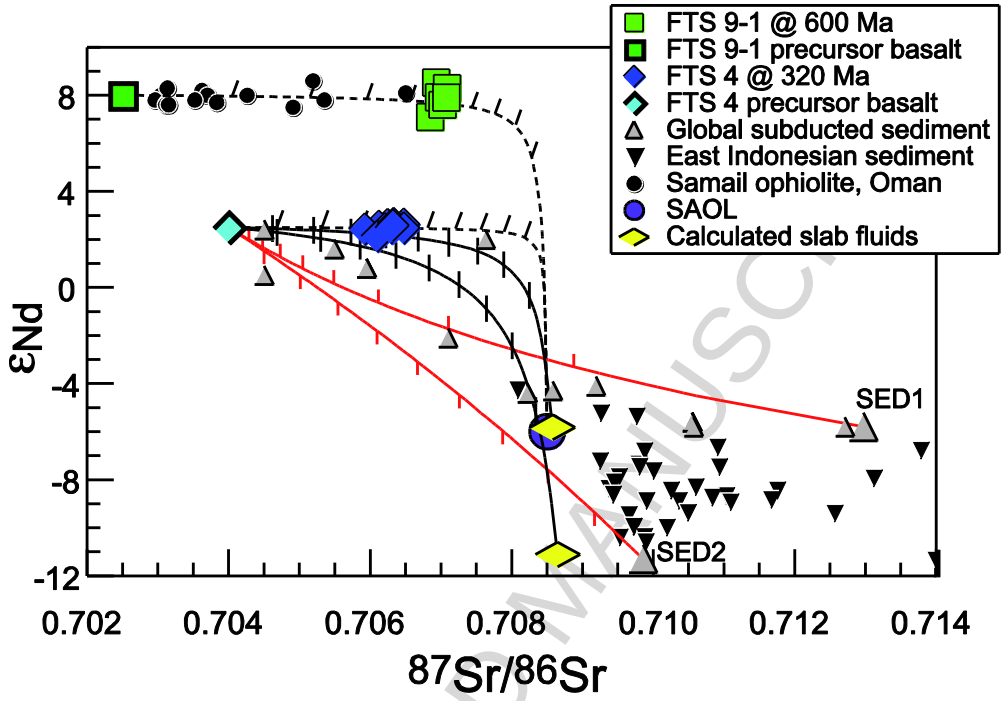

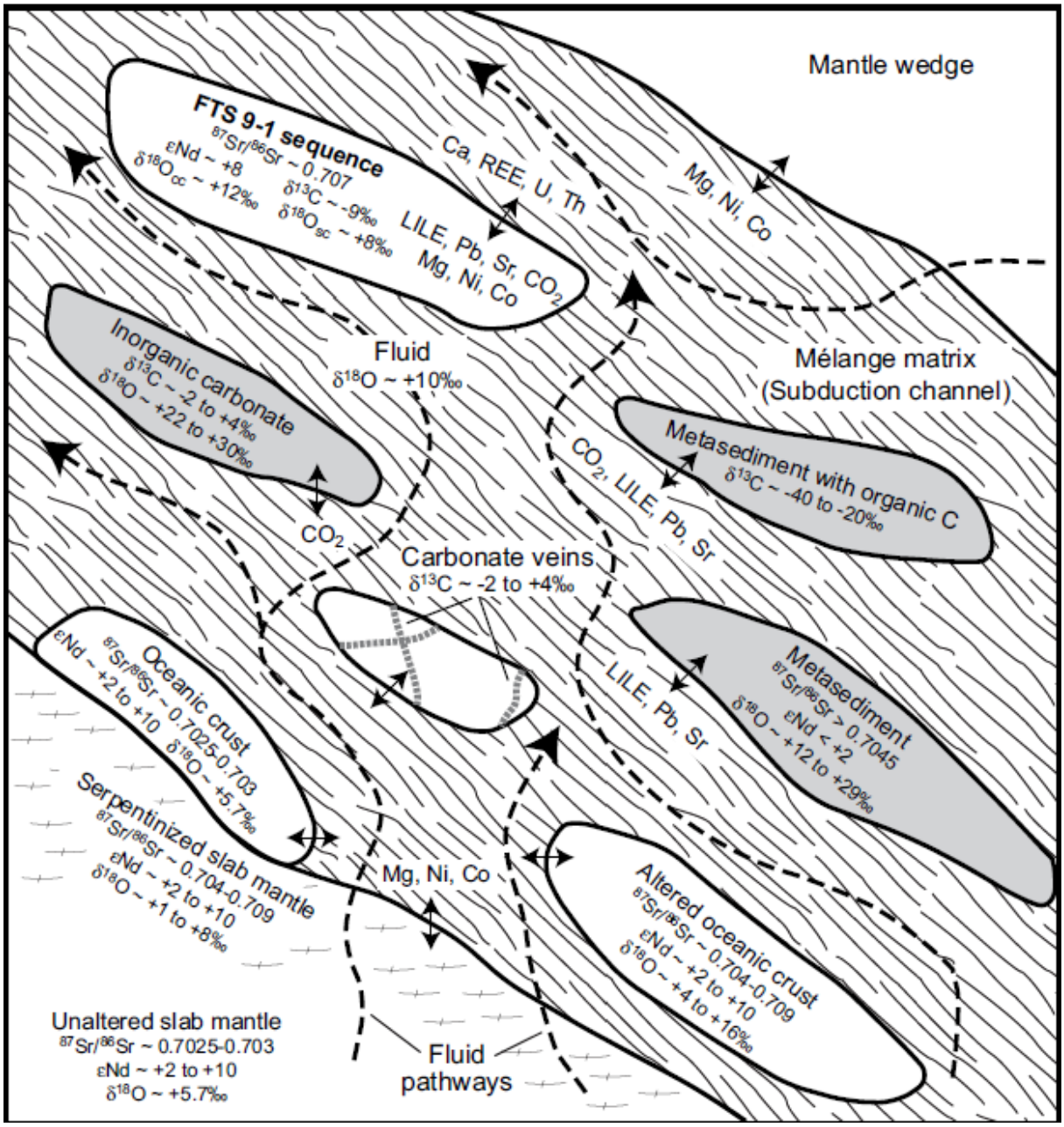

Fig. 12

Highlights

- Eclogites from the Tian Shan show blueschist-facies metasomatic overprint
- Fluid-induced metasomatism occurred at 320±11 Ma
- Fluid predominantly derived from seawater-altered oceanic lithosphere
- Carbonates reflect C sequestration of mixture of organic and inorganic components